

Scale invariance and dynamical correlations in growth models of molecular beam epitaxy

S. Das Sarma, C. J. Lanczycki,* R. Kotlyar, and S.V. Ghaisas†

Department of Physics, University of Maryland, College Park, Maryland 20742

(Received 26 May 1995)

Dynamical scaling behavior of the kinetic roughening phenomena in (1+1)- and (2+1)-dimensional models of molecular beam epitaxy (MBE) is studied using kinetic Monte Carlo simulations mostly within the solid-on-solid lattice gas approximation. We relate the simulation results of our finite temperature stochastic Monte Carlo algorithm, which employs local-configuration-dependent thermally activated Arrhenius diffusion, to those obtained from simpler manifestly nonequilibrium dynamical growth models involving instantaneous relaxation. The extracted critical exponents for kinetic roughening are found to be temperature dependent due to finite size and crossover effects, and in particular, the growth (β) and roughness (α) exponents decrease with increasing temperature as diffusion noise becomes stronger relative to the deposition noise. We find strong evidence for anomalous dynamic scaling, with global and local scaling behaviors being substantially different in 1 + 1 dimensions. Remarkably, the anomalous roughness exponent α' ($= \alpha$ in the *usual* dynamic scaling situation) defining the spatial scaling in the height-height correlation function is found to be approximately a temperature-independent constant (≈ 0.6 – 0.7 in 1+1 dimensions) in all our models, including the Arrhenius-activated diffusion model. An associated significant result is the marked up-down ($h \rightarrow -h$) asymmetry in our simulated growth morphologies, clearly indicating the presence of nonlinear microscopically irreversible processes dominating local growth features. We study in some detail the recently suggested connection between height fluctuations in MBE growth models and intermittent fluctuations in fluid turbulence by numerically calculating the multiaffine dynamic scaling behavior of higher moments of the height correlation functions and by obtaining the stretched exponential behavior of the step-height distribution functions in our growth models. We critically analyze our growth rules to comment on possible coarse-grained continuum descriptions that could qualitatively account for our MBE simulation results.

PACS number(s): 05.40.+j, 81.15.Hi, 82.20.Mj

I. INTRODUCTION

In molecular beam epitaxy (MBE) growth an atomic flux impinges upon a substrate which is held at a fairly high temperature (500–1000 K). The dynamically growing interface, where we restrict ourselves to idealized homoepitaxial MBE growth on flat singular surfaces along a specific crystallographic orientation of high symmetry, roughens kinetically due to the shot noise inherent in the incident beam. The basic physics of MBE growth involves a competition between deposition and diffusion—the noise due to diffusion being conserved and the deposition noise being nonconserved. Atomic diffusion smoothens the growth front, minimizing kinetic roughness, whereas deposition noise in most situations

generates interface roughness. The typical length scale over which diffusion produces smooth growth, the diffusion length, increases exponentially with increasing temperature (and decreases with increasing deposition rate) and at high temperatures and/or low deposition rates it is common to produce good-quality smooth thin films of very large areas with little kinetic roughness. This is the epitaxial layer-by-layer growth regime, which is of particular interest in materials science, and which has been extensively studied [1] using atomistic kinetic Monte Carlo simulations involving activated Arrhenius diffusion of surface atoms. The primary goal of these MBE growth simulations [1] has been to describe the smooth layer-by-layer epitaxial growth regime (possessing minimal kinetic roughness), and as such most of this earlier work was devoted to obtaining maximal information about the quality of the surface from observations of intensity oscillations from the specular beam in a reflected high energy electron diffraction (RHEED) experiment. Simulations were performed in the layer-by-layer growth regime to obtain various RHEED patterns by varying the input parameters such as substrate temperature, diffusion and evaporation rates, etc.

Based on these detailed simulational studies, a minimal kinetic Monte Carlo model [1,2] for studying MBE growth has emerged. This model has been shown to

*Permanent address: Computational Biosciences and Engineering Laboratory, Division of Computer Research and Technology, The National Institutes of Health, Bethesda, MD 20892.

†Permanent address: Department of Electronics Science, The University of Pune, Pune 411007, India.

be capable of producing reasonably accurate quantitative information about real MBE growth in the layer-by-layer growth regime. In this article, we use this minimal kinetic Monte Carlo model, involving local configuration-dependent-activated Arrhenius diffusion of surface atoms, to study MBE growth in the kinetically rough (as against epitaxial layer-by-layer) growth regime where deposition noise dominates diffusion noise. Here, adatom diffusion is ineffective in producing smooth films and permits the interface to roughen kinetically as the film grows due to the shot noise fluctuations in the incident beam. The signature of kinetic roughening imposing upon the layer-by-layer growth regime is an observed damping of the specular RHEED intensity oscillations. The region beyond the damped RHEED oscillations and the layer-by-layer growth regime, where the interface becomes rough and the surface is of poor quality from an experimental standpoint, has not been addressed in simulations until recently. Recent studies of idealized kinetically rough MBE growth models [2–5] have indicated that interface growth processes in general, and MBE in particular, can be viewed as examples of dynamical critical phenomena.

A question then naturally arises: What is the dynamical universality class of MBE growth? In spite of much work on this subject an unambiguous and widely accepted answer to this question has remained elusive. Our goal in this paper is to study in great detail the minimal kinetic Monte Carlo MBE growth model in an idealized situation in both one (which we shall denote as $d' = 1$ substrate dimensions, or $d = 1 + 1$ total spatial dimensions) and two ($d' = 2$ or $d = 2 + 1$ dimensions) substrate dimensions, and compare our numerical results to various proposed dynamical universality classes [3–22]. The idealizations we make (except where stated otherwise) are the solid-on-solid (SOS) approximation whereby no bulk vacancy or surface overhang is allowed to form during growth, neglect of desorption or evaporation from the growth front, ignoring any diffusion barrier (the so-called “Schwoebel barrier”) near step edges and any “hot-atom” or knockout effects [21] at the growth front. Surprisingly, these idealizations, instead of simplifying the identification of MBE growth universality, actually complicate matters and make the search for MBE growth universality more difficult and controversial. In particular, the “conserved” nature of our minimal model (i.e., no desorption, no vacancies or overhangs) rules out the generic nonlinear Kardar-Parisi-Zhang (KPZ) universality [20] which is now established [22] to be the asymptotic MBE growth universality class if one includes ballistic deposition and diffusion in the model (instead of the SOS model which we employ in the minimal model), which allows for overhangs and vacancies. Crossover effects in the ballistic model, however, show clear signs [19,22] of various SOS universality classes being studied in this paper. Inclusion of desorption or hot-atom effects is accepted by consensus to give rise to nonlinear KPZ or the linear Edwards-Wilkinson [18] behavior (EW) (i.e., the free-field KPZ without the nonlinearity). It is therefore somewhat surprising that the minimal MBE growth model [1–5] *without* the additional complications of va-

cancy and overhang formation, desorption, etc., is not yet completely understood from a kinetic roughening viewpoint whereas the more complicated situation is reasonably well understood, at least asymptotically, to be described [22] by the generic second-order KPZ growth universality. It is also becoming clear that the presence of a step-edge barrier within the SOS approximation leads to coarsening and pattern formation (with large “bumps” or “pyramids” on the surface) during growth [23,24]. Except in a few situations to be described below (where we show some ballistic deposition MBE simulation results for the sake of comparison with the minimal MBE model), we do not much discuss the roles of vacancies, overhangs, and desorption, assuming all of them to be negligible in our ideal SOS-MBE process which is taken to be well described by the minimal kinetic Monte Carlo growth model [1–5,25]. We largely neglect the Schwoebel diffusion barrier effect in this paper, taking the viewpoint that the situation without the step-edge barrier complications needs to be completely understood.

A number of simple, manifestly nonequilibrium models have been introduced [3,7–9,13,17] to represent MBE growth (to zeroth order) under far from equilibrium conditions. In these nonequilibrium dynamical growth models, deposited particles relax instantaneously after deposition according to some local microscopic rules. In real MBE growth (as well as in our minimal model) all the particles are allowed to move continuously after deposition, but depending upon the substrate temperature, growth rate, and individual atomic mobility, they may not equilibrate locally if the incident flux of atoms is relatively high and atomic diffusion is low. Understanding this low temperature and/or high deposition rate kinetic roughening regime is the motivation for the nonequilibrium dynamical models. (Complete equilibration of the growing surface configuration is obviously approached in the limit of zero growth rate and long growth times.) One of the motivations for introducing the “toy” models is eliminating conserved diffusion noise from growth simulations. We describe these various MBE-motivated nonequilibrium growth models later (Sec. III) in this paper, and one of our goals here is to relate the minimal MBE growth results to these dynamical models.

Quantitatively, dynamic scaling means that the growing surface exhibits generic scale invariance in both space and time. The assumption of a scale invariant surface implies a rescaling of the height $h(x, t)$ above the substrate upon a simultaneous rescaling of the coordinate $x \rightarrow bx$ and the time $t \rightarrow b^z t$ according to

$$h(x, t) \sim b^{-\alpha} h(bx, b^z t). \quad (1.1)$$

From this scaling form it is clear that when $\alpha \neq 1$ the directions parallel and perpendicular to the substrate are fundamentally distinct because they do not rescale in equivalent fashions. Such an anisotropy, however, seems well suited to the growth problem in general because the incident beam (assumed to be normal to the substrate) defines a special direction. When $\alpha < 1$, one calls such anisotropically scaling surfaces self-affine. Obviously then, if $\alpha = 1$ the height h and the lateral coordi-

nate x behave similarly and one recovers isotropic scaling of the surface height fluctuations. Based on this isotropy one may consider the growing interface to be a “surface fractal” [26] for $\alpha = 1$, where everywhere h varies linearly with position (usually in a piecewise fashion). We emphasize that unlike diffusion-limited aggregation (DLA), for example, neither the surface nor the entire aggregate for minimal SOS-MBE growth can be considered a self-similar fractal when $\alpha = 1$ since the bulk crystal contains no defects and is patently non-fractal.

The idea that growing interfaces exhibit generic dynamical scaling has held up well in nearly all models studied to date. The pair of dynamical exponents α and z and the associated exponent $\beta = \alpha/z$ by which one characterizes surfaces (i.e., its dynamical universality class), however, can vary based on the set of allowed microscopic processes. Knowing α and z for our minimal MBE model and comparing them to those obtained for the various nonequilibrium dynamical growth models should give us considerable insight into the dynamic scaling behavior and generic scale invariance aspects of MBE growth. One significant problem in this respect is the fact that the various simple nonequilibrium dynamical “toy” models which have been introduced in the context of MBE growth have themselves remained controversial and “unsolved” with respect to their asymptotic values of critical exponents α and z [10–16]. Thus, in addition to studying the minimal MBE growth model involving temperature-dependent-activated diffusion of all atoms at the growth front, we have carried out and report here detailed numerical simulations of a subset of the nonequilibrium dynamical models as well. A direct comparison of the minimal MBE model results with those of the nonequilibrium dynamical models tells us the extent to which specific “toy” models catch the MBE dynamic scaling behavior.

Ultimately, however, one wishes to relate the simulated critical exponents (α, z , etc.) of our minimal MBE growth model to those derived theoretically for a coarse-grained continuum differential equation (e.g., EW, KPZ equations) for the height fluctuations. There is no rigorous proof that this can be done in all situations, but if α and z exist, there is good reason to believe that a long-wavelength continuum coarse-grained differential equation description should apply asymptotically. In the MBE growth problem, the search for the continuum equation has been severely hampered by crossover effects, and, in our opinion, a large number of recent experimental results claiming agreement with one or the other existing continuum equation in the literature has added to this confusion. We will, throughout this article, make connections between our numerical results and the exponents obtained analytically for various continuum MBE growth equations. We warn the reader, however, that in spite of our rather extensive simulations a complete picture for the asymptotic universality class of the minimal MBE model, even in $d = 1 + 1$ dimensions, does not emerge. It should also be emphasized that the search for the universality class of MBE growth (and for the associated MBE growth equation) is not just an academic exercise. If MBE growth universality is such that $\alpha = 0$ (as it would

be in $d' = 2$ for the EW universality class), then real MBE growth is smooth (more precisely, only logarithmically rough) as a matter of principle. On the other hand, if $\alpha \neq 0$ in MBE growth, then the smooth layer-by-layer growth regime is only a finite size transient, and asymptotically MBE growth is always kinetically rough. Thus understanding the MBE dynamical universality class is of some technological importance in determining optimum conditions for the growth of smooth high-quality thin films.

One gains physical insight into interface growth dynamics by comparing the scaling exponents with those predicted analytically from the asymptotic properties of various stochastic differential equations believed to describe the long-wavelength characteristics of various growth processes [3,5–9,18,20,27]. The goal is to use the continuum equations to predict scaling behavior, and hence provide a statistical picture of the time development of surface morphology. The statistical properties of interface height fluctuations are manifestations of the specific dynamic scaling behavior of the problem. Global roughness of a surface is measured by its width, or root-mean-square fluctuation about the average height; local roughness can be quantified by computing the height-height correlations in space and time (see Sec. II). Surprisingly, it has become increasingly clear recently that the local and global dynamic scaling behaviors are distinctly different (at least in $d' = 1$) for the class of surface-diffusion-driven nonequilibrium dynamical models which were introduced in the context of understanding MBE growth. This “anomalous scaling” behavior is not predicted by the simplest dynamic scaling ansatz [17] and will be explored in some detail in this article.

Our goal is to develop an understanding of dynamical correlations in the interface kinetic roughness of the growing thin film, and as such we pay particular attention to the dynamical height-height correlation function and its higher moments. In some situations we also directly compute the structure factor, which is related to the Fourier transform of the height-height correlation function. The interface width, which is the root-mean-square height fluctuation averaged across the whole substrate, measures the global kinetic roughening properties, and is simply related to the “diagonal” component of the height-height correlation function which probes the details of local roughening. We find that MBE growth in $d = 1 + 1$ follows anomalous dynamic scaling with the dynamical critical exponents for local roughening as determined by the height-height correlation function being decisively different from those determined from the global scaling of the interface width. Our MBE growth results in $d = 2 + 1$ also exhibit anomalous dynamic scaling, but the necessarily smaller size of these simulations prevent us from making a decisive conclusion for $d' = 2$.

The rest of this paper is organized as follows. In Sec. II we discuss the fourth-order conserved continuum growth equation which has been introduced as a possible coarse-grained large-scale description for MBE growth. In Sec. III we describe the various growth models studied in this paper. In Sec. IV we present and discuss our numerical results, and we conclude in Sec. V. Unless other-

wise stated all our numerical simulation results, both for the temperature-dependent-activated hopping stochastic MBE models and the instantaneous-relaxation nonequilibrium dynamical growth models, are SOS results for $d = 1 + 1$ growth. We present some limited $d = 2 + 1$ growth results and a few representative MBE ballistic deposition results as well.

II. THEORY

We are studying the generic scale invariance properties of stochastic Arrhenius hopping MBE growth models. Ideally this involves three steps: (i) showing that the simulation results of the minimal MBE growth model obey the dynamic scaling hypothesis; (ii) connecting the dynamical growth exponents obtained in step (i) with those in some well-defined instantaneous-relaxation discrete growth models; (iii) connecting these instantaneous-relaxation discrete growth models (which provide consistent descriptions of the minimal MBE growth model) to coarse-grained continuum differential equations whose critical exponents can, in principle, be theoretically calculated. Note that step (ii) is necessary because even the minimal MBE growth model involves both diffusion and deposition noise as well as several different hopping rates (corresponding to the initial number of bonds of the hopping atom), and therefore may suffer from severe crossover effects, which should, in principle, be substantially reduced in the instantaneous-relaxation models.

The continuum coarse-grained differential equations must be consistent with the translational invariance in the growth direction and rotational invariance in the substrate plane. If desorption, overhangs, vacancies, etc. are allowed then the leading-order growth equation is the generic Kardar-Parisi-Zhang equation [20]

$$\partial h / \partial t = \nu_2 \nabla^2 h + \lambda_2 |\nabla h|^2 + \eta(\mathbf{x}, t), \quad (2.1)$$

which has been much discussed in the literature. [We write our growth equations for the dynamical height fluctuation $h(\mathbf{x}, t)$ subtracting out the uniform growth term due to the average incident flux; all coordinates h and \mathbf{x} are treated as dimensionless quantities after normalizing by the physical lattice constants in either direction.] The noise η throughout this paper is a spatio-temporal noise, $\eta = \eta_F + \eta_D$, where noise has the correlators $\langle \eta_F(\mathbf{x}, t) \eta_F(\mathbf{x}', t') \rangle = 2N_F \delta^{d'}(\mathbf{x} - \mathbf{x}') \delta(t - t')$ and $\langle \eta_D(\mathbf{x}, t) \eta_D(\mathbf{x}', t') \rangle = -2N_D \nabla^2 \delta^{d'}(\mathbf{x} - \mathbf{x}') \delta(t - t')$. By definition the noise has zero mean so that $\langle \eta_F(\mathbf{x}, t) \rangle = \langle \eta_D(\mathbf{x}, t) \rangle = 0$. In this description, η_F and η_D are the random Gaussian white noise arising from the fluctuations in the external deposition flux and in the hopping diffusion, respectively. The coefficients N_F and N_D are the respective strengths of the unconserved deposition noise η_F and the conserved diffusion noise η_D . The asymptotic critical exponents are determined by the nonconserved part of the noise η_F , while η_D is asymptotically irrelevant in the presence of nonzero η_F in the renormalization group sense. We emphasize, however, that for length scales $x < l$, where l is the diffusion length [28], η_D may introduce crossover effects and in particular, η_D

may determine the effective exponents in the minimal MBE growth model at short length scales and at high temperatures when l is large. Because we are interested in the asymptotic universality class of MBE growth we consider the noise η to be unconserved deposition noise from now on unless stated otherwise. Consistent with the standard practice we take the shot noise to be uncorrelated random white noise.

It is well accepted that unconserved growth (either due to desorption or due to vacancy or overhang formation) is asymptotically described by the KPZ equation. Our ballistic deposition-activated diffusion MBE growth simulation results (some of which are presented in Sec. IV of this paper) are consistent with an asymptotic KPZ universality even though we also see clear indications of conserved growth universalities in the preasymptotic crossover regime [22]. But our main goal in this paper is understanding the minimal MBE growth model which is based on the desorption-free SOS model because under the usual MBE growth conditions evaporation from the growth front and vacancy and overhang formation are thought to be negligibly small. Then, apart from the incoming flux, growth must obey a current conservation law defined by

$$\partial h / \partial t = -\nabla \cdot \mathbf{j} + \eta(\mathbf{x}, t), \quad (2.2)$$

where \mathbf{j} is the conserved surface mass current. We emphasize that the generic KPZ nonlinearity is ruled out by the conservation law defined in Eq. (2.2) because $|\nabla h|^2$ cannot be expressed as a divergence. Following Lai and Das Sarma [8] the most general continuum growth equation which preserves current conservation and all the symmetries of the problem (namely, translational invariance along the growth direction and rotational invariance in the substrate plane), can be written as

$$\begin{aligned} \partial h / \partial t = & \nu_2 \nabla^2 h - \lambda_4 \nabla^4 h + \lambda_{22} \nabla^2 (\nabla h)^2 \\ & + \lambda_{13} \nabla (\nabla h)^3 + \eta(\mathbf{x}, t), \end{aligned} \quad (2.3)$$

with the corresponding surface mass current having the form

$$\begin{aligned} \mathbf{j} = & -\nu_2 \nabla h - \lambda_{13} (\nabla h)^3 + \nabla [\nu_4 \nabla^2 h - \lambda_{22} (\nabla h)^2] \\ = & -(\nabla h) \{ \nu_2 + \lambda_{13} |\nabla h|^2 \} + \nabla \{ \nu_4 \nabla^2 h - \lambda_{22} |\nabla h|^2 \}, \end{aligned} \quad (2.4)$$

where ν_2 , ν_4 , λ_{22} , and λ_{13} , the macroscopic growth coefficients, are in principle determined by the growth conditions (e.g., temperature, diffusion length, flux rate) and by the microscopic energetic and kinetic parameters describing the substrate and the growing system. For our purposes ν_2 , ν_4 , λ_{22} , λ_{13} are simply parameters of the long-wavelength coarse-grained continuum theory. Note that the current \mathbf{j} is written as a sum of two terms in Eq. (2.4), the first of which arises from a generalized surface tension and the second term arises from a generalized (nonequilibrium) chemical potential.

If $\nu_2 \neq 0$, then the long-wavelength, long-time dynamical critical properties of Eq. (2.3) are necessarily determined by the first term $\nu_2 \nabla^2 h$ in the right hand side, and all the other (fourth-order) terms are irrelevant from a renormalization group viewpoint. The fourth-order terms may contribute to crossover effects (thereby being a potential complication for experimental, as well as simulational, results), but do not alter the asymptotic growth exponents. The continuum equation without the fourth-order terms in Eq. (2.3), the EW equation [18], has been much studied in the literature:

$$\partial h / \partial t = \nu_2 \nabla^2 h + \eta(\mathbf{x}, t). \quad (2.5)$$

In the absence of the $\nu_2 \nabla^2 h$ EW term (i.e., $\nu_2 = 0$) the most relevant fourth-order term in Eq. (2.3) is the nonlinear $\lambda_{13} \nabla(\nabla h)^3$ term, which has recently been shown [29,30] to behave equivalently to EW universality because it automatically generates the $\nabla^2 h$ linear term upon renormalization. While the generation of the second-order $\nabla^2 h$ linear term from the fourth-order $\nabla(\nabla h)^3$ nonlinearity is now established [30] theoretically, this result may be motivated by the following two simple observations: (1) The $\nabla(\nabla h)^3$ nonlinearity can be expressed as

$$\nabla(\nabla h)^3 = 3(\nabla h)^2(\nabla^2 h), \quad (2.6)$$

so that

$$\nu_2 \nabla^2 h + \lambda_{13} \nabla(\nabla h)^3 = \nu_2(\nabla^2 h) \left\{ 1 + \frac{3\lambda_{13}}{\nu_2} (\nabla h)^2 \right\}, \quad (2.7)$$

implying the generation of the $\nabla^2 h$ term upon renormalization of the $\nabla(\nabla h)^3$ term. (2) The $\nabla^2 h$ and the $\nabla(\nabla h)^3$ terms are generated as the first two terms in an expansion if one considers a dynamical Langevin equation based on the simple surface tension Hamiltonian:

$$\mathbf{H} \sim \int d\mathbf{x} \sqrt{1 + (\nabla h)^2}, \quad (2.8)$$

$$\sim \int d\mathbf{x} \left[1 + \frac{1}{2}(\nabla h)^2 - \frac{1}{8}(\nabla h)^4 + \dots \right], \quad (2.9)$$

again implying that the $\nabla(\nabla h)^3$ term is, in effect, a higher-order correction to the EW $\nabla^2 h$ term. The $\nabla(\nabla h)^3$ growth nonlinearity was introduced [8] by Lai and Das Sarma, and has recently been rediscovered [23,31] in the context of slope selection in surface coarsening for unstable growth under a step-edge diffusion barrier (Schwoebel barrier).

It has been argued [8,9] that the most relevant second-order EW term $\nabla^2 h$ is absent for MBE growth on flat substrates ($\nu_2 = 0$), and most numerical simulations are at least consistent with the scenario that $\nu_2 \approx 0$ if not $\nu_2 = 0$. Our discussion of MBE growth simulations under SOS conditions will therefore be based on Eq. (2.3) as well as [33] its purely fourth-order variant [8,9] with $\nu_2 = \lambda_{13} = 0$:

$$\partial h / \partial t = -\lambda_4 \nabla^4 h + \lambda_{22} \nabla^2(\nabla h)^2 + \eta(\mathbf{x}, t). \quad (2.10)$$

It is also useful to consider [3,6,7] the purely linear fourth-order conserved growth equation [$\lambda_{22} = 0$ in Eq. (2.10)]:

$$\partial h / \partial t = -\lambda_4 \nabla^4 h + \eta(\mathbf{x}, t), \quad (2.11)$$

which is the nonconserved version of the Mullins-Herring surface-diffusion equation [32]. For the sake of completeness we also write down [8] the complete fourth-order conserved growth equation [i.e., $\nu_2 = 0$ in Eq. (2.3)], which follows [29,30] the EW asymptotic behavior:

$$\partial h / \partial t = -\lambda_4 \nabla^4 h + \lambda_{22} \nabla^2(\nabla h)^2 + \lambda_{13} \nabla(\nabla h)^3 + \eta(\mathbf{x}, t). \quad (2.12)$$

In Table I we provide the theoretically known critical growth exponents α , β , and z in both $d = 1 + 1$ and $d = 2 + 1$ for the relevant growth equations. The linear growth equations, Eqs. (2.5) and (2.11), are trivially soluble via Fourier transformation whereas the analytical results for the nonlinear equations are obtained via the dynamical renormalization group (DRG) technique [8,20,30].

Conceptually the simplest and most relevant continuum SOS growth equation is obviously Eq. (2.5), the EW equation, which dominates the long-wavelength scaling properties if $\nu_2 \neq 0$. The chief physical effect captured in the derivation of this equation is the relaxation of atoms to local height minima: growth which is found to scale in the same manner as the EW equation is thus thought to be asymptotically driven by the transfer of matter to the lowest local positions on the surface via an effective surface tension (or, effective gravity). Notable deviations from this simplest of descriptions have, however, been seen in MBE growth simulations and in a class of MBE-inspired instantaneous-relaxation discrete growth models. These models contain different physics because the atoms are driven not to local height minima, but to local sites providing a higher number of bonds or local coordination number (see Sec. III for details), which is expected to be more relevant to real MBE. This new class of surface-diffusion-driven models develops interface fluctuations which seem to be better described [3–10] by

TABLE I. Theoretical asymptotic exponents for various continuum equations discussed in the text, listed according to the term dominating the asymptotic scaling of the given equation. The exponents for Eq. (2.1) in 2+1 are estimates from simulation, and those for the $\nabla(\nabla h)^3$ term are obtained [8] from a Flory-type dimensional analysis but are known [28] to only be transients prior to a crossover to the universality of Eq. (2.5). All other exponents are either exact, or accurate to at least a two-loop DRG calculation.

Dimension Exponent	1 + 1			2 + 1		
	α	z	β	α	z	β
$\nabla^2 h$ —Eq. (2.5)	1/2	2	1/4	0 (log)	2	0 (log)
$(\nabla h)^2$ —Eq. (2.1)	1/2	3/2	1/3	~ 0.4	~ 1.67	~ 0.24
$\nabla^4 h$ —Eq. (2.11)	3/2	4	3/8	1	4	1/4
$\nabla^2(\nabla h)^2$ —Eq. (2.10)	1	3	1/3	2/3	10/3	1/5
$\nabla(\nabla h)^3$ —Eq. (2.12)	3/4	5/2	3/10	1/2	3	1/6

the fourth-order continuum growth equation in Eq. (2.10) or (2.11), at least over a large range of system sizes and growth times.

A difficult conceptual feature of $d = 1 + 1$ models described by Eqs. (2.10) and (2.11) is that the interface height fluctuations can, in the thermodynamic limit $L \rightarrow \infty$, possess an amplitude growing as fast or faster than the system size L . This implies that on no scale can the interface be considered smooth in the sense that the roughness exponent $\alpha \geq 1$. This statement implicitly assumes a statistical physics viewpoint because the thermodynamic limit is being considered. When viewed on much smaller scales $x \ll L$ (the so-called solid state physics viewpoint [34]), larger values of α instead imply locally smoother surfaces [34]. Within this finite size “solid state physics” viewpoint, self-affine surfaces with smaller α (< 1) tend to have a rougher, more jagged appearance than super-rough ($\alpha \geq 1$) interfaces because the lateral scale of a typical super-rough fluctuation is large with little residual roughness *on small length scales*. When discussing roughness in this article, however, we take the long-wavelength, statistical physics viewpoint where larger α means a rougher surface unless explicitly noted.

The isotropy occurring for $\alpha = 1$ (where $h \propto x$) can be considered to define [26] a borderline growth regime separating the anisotropic cases of self-affine surfaces ($\alpha < 1$) from the super-rough, nonfractal regime ($\alpha > 1$). As we discuss in later sections, very large height fluctuations which are generically observed on super-rough surfaces (see Fig. 9 below) appear to be responsible for such large global roughness exponents ($\alpha > 1$). We explicitly demonstrate, however, that the local roughness exponent α' is less than or equal to unity for all $\alpha \geq 1$. In geometrical terms, in the self-affine case the initial overall orientation of the substrate does not change during growth while for $\alpha = 1$ the height is linear with position so the flat initial surface assumes a new global orientation. In the super-rough case, groove formation can be viewed as a *local* orientational instability which results in values of $\alpha > 1$. Both $\alpha = 1$ and $\alpha' = 1$ should hold for completely isotropic growth, which may be the situation, within logarithmic correction, for the continuum equation (2.10).

Morphologically, then, super-rough surfaces are much rougher than those obeying the EW equation, showing very large steps and deep grooves in the interface (see examples below and in Refs. [5,7,14,15]). In the long-time limit, though, some [7] of these discrete models are believed to cross over to the EW equation [10,12,16,35]. The discrete growth model introduced by Das Sarma and Tamborenea [3,5], the so-called DT model, which we believe to be the relevant dynamical model underlying the minimal MBE growth simulations, has shown no such crossover to EW universality [10,11,14]. The DT model exhibits scaling properties tantalizingly similar to those of the linear Eq. (2.11), but with very significant differences [11,14]. In particular, the recently discovered [11,12] anomalous time dependence of the correlation function in the DT model cannot be explained by Eq. (2.11). Recently, Krug has pointed out [14] a number of peculiarities in higher moments of the height-height

correlation functions in the DT model. While these peculiarities can be thought of as the higher-order manifestations of anomalous dynamic scaling, there are some interesting analogies [14] to the phenomenon of intermittency in fluid turbulence which we explore in more detail in this paper. We show that many characteristics of the DT model, including most of these peculiarities, are indeed reflected in the stochastic, temperature-dependent minimal MBE growth model.

Several examples of stochastic MBE growth models allowing for temperature-dependent kinetics with no evaporation have recently appeared in the literature in the context of dynamical scaling studies [4,5,22,25,36–38]. There have also been attempts [21] to derive an equation of motion for MBE growth using a master equation approach defining the transition probabilities in terms of kinetic rates, with the conclusion that Eq. (2.10), the so-called Lai–Das Sarma–Villain (LDV) equation, is the appropriate continuum equation describing MBE growth. Under SOS restrictions one generally observes that the scaling exponents are dependent on temperature and on the details of the microscopic hopping rules [4,5,25,36]. Simulations relaxing the SOS restriction by using ballistic deposition (BD) and diffusion [22,37,38] (i.e., permitting overhangs and vacancies when atoms land or move upon the surface) show an initial temperature-dependent SOS-like transient regime which asymptotically crosses over to scaling typified by the KPZ equation, Eq. (2.1).

The kinetically roughening interface can be characterized by extracting exponents from the evolving surface width or from the dynamical height-height correlation function; recently the actual form of the scaling function in such models has been studied directly in several idealized dynamical models [11,12,14]. There has been less discussion of the dynamical scaling function of finite temperature, stochastic growth models. We present in this paper such an analysis of stochastic growth models with activated hopping in $1+1$ and $2+1$ dimensions, analyzing the scaling function underlying the height-height correlation function $G(x, t)$ in the context of the anomalous scaling hypothesis proposed recently [11,12]. We further analyze these models for multifractal intermittent behavior [14,39] and show that the minimal SOS-MBE model possesses two distinct characteristics of the DT model, namely, anomalous dynamic scaling *and* multifractality. We also present extensive results on multiscaling in several instantaneous-relaxation discrete growth models permitting a critical comparison with the minimal MBE model results.

III. MODELS

Before discussing the details of our models, we define the quantities used to characterize the growing surfaces. The most obvious and common measure of the height fluctuations of an interface is given by the width W , or the root-mean-square fluctuations in the surface height $h(\mathbf{x}, t)$: $W^2(L, t) = \{\sum_{\mathbf{x}} [h(\mathbf{x}, t) - \bar{h}(t)]^2 / L^d\}$, where L is the linear substrate size and $\bar{h}(t)$ is the average height, and we also perform an ensemble average over several re-

alizations of the simulation. The scaling hypothesis implies that the width scales as $W^2(L, t) \sim L^{2\alpha} g(L/t^{1/z})$, where the asymptotic properties of the scaling function are $g(y) \rightarrow \text{const}$ for $y \rightarrow 0$ and $g(y) \rightarrow y^{-2\alpha}$ for $y \rightarrow \infty$. For short times such that the correlation length $\xi \sim t^{1/z}$ is small compared with the system size ($\xi \ll L$), then $W(L, t) \sim t^\beta$, with the exponent $\beta = \alpha/z$. Notice that the global length scale L dictates the behavior of W in the large t limit ($t > L^z$), and that the fluctuations are measured with respect to the globally averaged height of the interface.

The height-height correlation function is calculated using the definition $G(x, t) = \langle [h(\mathbf{x} + \mathbf{x}_o, t) - h(\mathbf{x}_o)]^2 \rangle_o$, where $\langle \rangle_o$ denotes both averaging over \mathbf{x}_o and multiple realizations of the model. In the usual (i.e., nonanomalous) dynamical scaling situation the growing surface is self-affine, implying that the correlation function $G(x, t)$ for interface growth varies with the local scale x at time t as

$$G(x, t) \sim x^{2\alpha} g(x/\xi(t)), \quad (3.1)$$

with $\xi(t) \sim t^{1/z}$ and where the asymptotic behavior of $g(y)$ is identical to that shown above. This form follows from the hypothesis that the surface is a self-affine object. The scaling function $g(y)$ can be found by plotting $G(x, t)/x^{2\alpha}$ vs y , and for $y = x/t^{1/z} \ll 1$ one expects that $g(y)$ will saturate to a constant, implying generic scale invariance and self-affinity. Finally, we measure the structure factor $S(k)$ of the surface, which is related to the Fourier transform of $G(x, t)$ at large times when the interface has reached saturation. Specifically, $S(k) = \langle h(k)h(-k) \rangle$, where $h(k)$ is the Fourier transform of the height profile, and the angular brackets here denote an ensemble average in the limit of large times. The relevant scaling behavior of the structure factor is $S(k) \sim k^{-\gamma}$, for $k > 1/\xi$, which for the saturated interface ($\xi \sim L$) holds at all k in the simulation.

As emphasized previously, the usual dynamic scaling does not hold for MBE growth in $d = 1 + 1$, with anomalous dynamic scaling and multifractality showing up dramatically. In the context of multifractality (or more specifically, multiaffinity [14,39]), a generalized correlation function proves useful, defined through the various moments of the height difference:

$$G_q(x, t) = \langle |h(\mathbf{x} + \mathbf{x}_o, t) - h(\mathbf{x}_o)|^q \rangle_o^{1/q}. \quad (3.2)$$

[Note that we have included the q th root in the definition of G_q , while it is *not* included in the definition of G in Eq. (3.1).] For a truly self-affine object, the functions G_q have q -independent scaling exponents, while q dependence is the hallmark of multifractality. Also relevant will be the step-height distribution function parametrized by the form $P(s) \sim \exp(-as^\delta)$, where $s = h(x+1) - h(x)$. In the case of a self-affine surface growing under the influence of δ -function-correlated white noise, large steps are rare and $\delta = 2$ so that $P(s)$ is Gaussian [14,40]; multiaffine surfaces show a stronger tail to the distribution, corresponding to the presence of more high steps, and $\delta < 2$. We note that the function $G(1, t)$ is the mean square step height, and thus the second moment of $P(s)$.

For the usual dynamic scaling behavior $G(1, t)$ quickly saturates and becomes a constant as $\xi \gg 1$ whereas for anomalous scaling, $G(1, t) \sim t^{\kappa/z}$ with κ the anomalous scaling exponent introduced in Ref. [11].

In addition to our stochastic MBE model, we will have occasion to refer to many dynamical growth models possessing instantaneous relaxation, which we discuss in the following subsection.

A. Dynamical SOS models

In all of these models, the deposition process is identical and obeys the SOS restriction: a randomly chosen substrate coordinate x is selected, and the height $h(x, t)$ of the interface above that site is incremented by one. All sites below the newly incorporated site are occupied due to the SOS constraint. The time t is measured in number of layers deposited, and the deposition rate in all cases is fixed at 1 layer/sec. When there is no diffusion of deposited atoms (the random deposition model, RD), the columns grow in an uncorrelated manner and the individual heights are drawn from a Poisson distribution ($\beta = 1/2$; α and z are undefined because there are no lateral correlations and $\xi \rightarrow 0$).

1. Family model

The simplest way to add relaxation was studied by Family [17] in a simulation that serves as a paradigm for the behavior of self-affine growth models following the scale invariant features of the EW equation and Eq. (3.1). Relaxation was included simply by comparing the height at the deposition site with the height at the nearest neighbor sites: if at a local height minimum the particle remains at the deposition site, otherwise the particle relaxes to the location with the minimum height [Fig. 1(a)]. That atom has no further mobility and is considered part of the bulk for the remainder of the simulation. Thus the relaxation is instantaneous and complete following random deposition events. For reference, the dynamical exponents expected for models following the EW equation are (see also Table I) $z = 2, \alpha = (3 - d)/2$. The simulations of the discrete Family model are completely consistent with these exponents in $d = 2$ and 3. Note that a generalization of the Family model where the instantaneous relaxation to local height minima occurs over a finite ‘‘diffusion’’ length (rather than just over the nearest neighbors) also asymptotically belongs to the EW universality class.

2. DT, Wolf-Villain, and related models

In the Wolf-Villain (WV) [7] model a deposited atom on the surface is allowed to relax to a nearest neighbor site if it can increase its number of bonds (a bond being made to each occupied nearest neighbor site). Furthermore, the atom will choose the site which provides the

maximal coordination if multiple options exist. There are no restrictions on the initial bonding state. It is important to distinguish this model from the very similar DT model [3], in which deposited atoms still relax to nearest neighbor sites (with greater bonding) but only when the deposition site has no occupied *lateral* nearest neighbors. Also in contrast with WV, the diffusing DT atom always chooses randomly among several possible landing sites with higher bonding configurations, not always selecting the site providing the maximum number of bonds. Thus DT only increases coordination (provided the initial coordination is one) whereas WV tries to maximize coordination (independent of the initial coordination number). Figures 1(b) and 1(c) explicitly display the differences in the relaxation rules between WV and DT. We note that these rules make no allowance for height minimization, although it often implicitly occurs as more highly coordinated sites tend to correlate with sites at a minimum local height. But, importantly, this is not always the case, as illustrated by atoms *e*, *f* in Figs. 1(b) and 1(c). As noted previously, in $d = 1 + 1$, both models show scaling behavior indicative of Eq. (2.11), for which $z = 4, \alpha = (5 - d)/2$. Recent work in $d = 2 + 1$ [35] has

shown the WV model to follow Eq. (2.10), generating the more relevant fourth-order nonlinear term $\nabla^2(\nabla h)^2$ for which $z = (7 + d)/3, \alpha = (5 - d)/3$ [8]. Measurement of the tilted-substrate surface current, however, indicates that all of this may be a transient [16] and that the asymptotic WV scaling is given [35] by the EW equation. The DT model therefore remains the only simple dynamical SOS growth model which has not yet been demonstrated to asymptotically cross over to the EW behavior. In fact, surface current measurements on tilted substrates and symmetry arguments [41] suggest that the asymptotic scaling behavior of the DT model cannot be described by the EW equation.

We propose two extensions of the DT model. First, we generalize the model to allow atoms to search up to D sites away for the nearest kink site, introducing the variable diffusion length D (the original model simply having $D = 1$). In addition, we have allowed for atoms to experience delayed hopping (within the $D = 1$ model). A new atom upon deposition relaxes according to the rules of the normal DT model. If the incorporation of this new atom creates a kink site within $D = 1$ units of *any old* surface atoms with no lateral bonds, the old atom

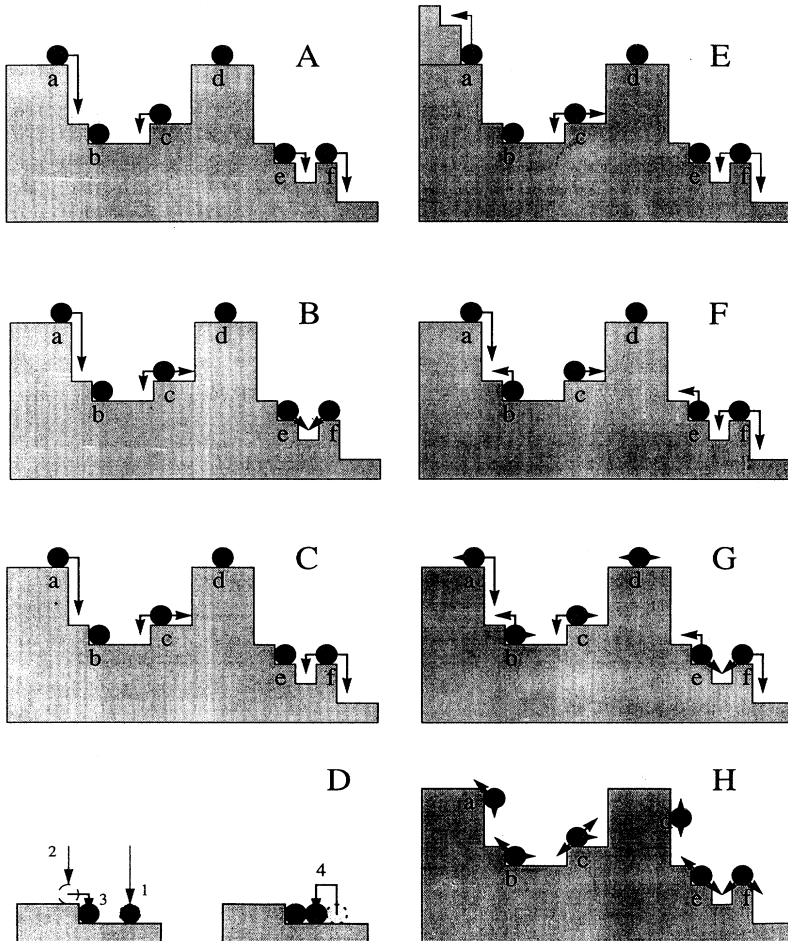


FIG. 1. Schematic configurations defining the growth rules for various models discussed in this paper in $1 + 1$ dimensions. (a) Family model, (b) Wolf-Villain (WV), (c) Das Sarma-Tamborenea (DT), (d) time-dependent hopping (TDH) modification to the DT model, (e) Lai-Das Sarma (LDS), (f) larger curvature model (LC), (g) the minimal MBE model, i.e., the stochastic growth model in solid-on-solid approximation (SOS-MBE), (h) stochastic ballistic deposition model (BD). Atom *a* in (e), while hopping up in the modified configuration, would not move in DT, and hops down in LC.

moves to the newly created kink site [Fig. 1(d)]. We call this the time-delayed hopping (TDH) model. The time-delayed hopping contained here encourages the formation of large islands on flat surfaces rather than many small ones, and allows atoms to interact with their changing environment.

Other models can be obtained with further modifications of DT-WV rules [10]. First, note that in 2+1 dimensions on a cubic lattice, a deposited atom can have at most five nearest neighbors and still relax in a SOS model. A model can be named [10] depending upon the maximum number of bonds that are allowed to break when relaxing by finding a more highly coordinated site. Thus, e.g., a 3+ model means that if an atom on deposition possesses no more than three bonds then it is allowed to hop to a nearest neighbor site if it can increase its number of bonds. An atom with four bonds on deposition is not allowed to move in the 3+ model. When multiple relaxation sites are present, one is selected randomly. In this notation the DT model becomes “1+” and the WV model is close to “2+.”

3. Lai–Das Sarma model

This model, while also similar to the DT and WV models, has important differences. Atoms with no lateral bonds relax exactly as in the $D = 1$ DT model; atoms with a single lateral bond (i.e., at a kink site) move to the nearest kink site with a smaller step height [8] [Fig. 1(e)]. The latter rule allows for upward motion of atoms, in contrast to previous models. Lai and Das Sarma (LDS) [8] found this model to obey Eq. (2.10) in $d = 1 + 1$ [8].

4. Larger curvature model

The last model in this class is the so-called “larger curvature” (LC) model introduced by Kim and Das Sarma [13]. Rather than making height differences or bonding the criteria for relaxation, this model explicitly calculates the curvature $[h(x+1) + h(x-1) - 2h(x)]$ at a randomly chosen site x and at all of its nearest neighbors. The

particle then relaxes to that site with the larger curvature, ties being decided randomly (unless the site x is involved, whereby the particle does not relax), as depicted in Fig. 1(f). Using an argument based on a Hamiltonian proposed for this model [13], the LC model can be shown to exactly obey the simple linear ∇^4 universality of Eq. (2.11), whether measured by the W , G , or $S(k)$. Thus the asymptotic behavior of the Family and the LC model are exactly known to be described by Eqs. (2.5) and (2.11), respectively, whereas the WV model shows long-time transients somewhat similar to Eq. (2.11) and is thought to cross over asymptotically to the behavior of Eq. (2.5).

B. Stochastic SOS model

This is the minimal MBE growth model which is constructed to simulate the spirit of real MBE growth by including the effects of temperature-dependent activated diffusion of adatoms with rates that depend upon the local bonding configuration. The deposition of atoms occurs in the same manner as in the dynamical models detailed in the preceding section. Also as in the dynamical models, relaxation of an atom is allowed only to nearest neighbor sites. However, the diffusional processes are more complicated in that any atom (not just the most recently deposited atom) at the surface may hop at any time (not only at the time of its deposition), with a rate depending on the number of bonds it possesses at that time. In order to respect detailed balance, the atomic hopping rate is independent of the height difference between columns, and there are *no* requirements that each hop must increase the coordination of the hopping atom [Fig. 1(g)]. Hops which decrease the number of bonds can occur, but the hopping rates are such that atoms landing in weakly bound sites will subsequently relax with an exponentially enhanced rate so that in a statistical sense atoms reside for the longest times in tightly bound locations, getting permanently incorporated when covered by other atoms. Note that a hopping atom is allowed to go either up or down in this model.

TABLE II. Diffusion rates at several temperatures for the minimal SOS-MBE model. Given is R_n/R_D for $d = 2, 3$, where the deposition rate $R_D = 1$ layer/sec and R_n is the activated hopping rate for an atom with n bonds as defined in the text. The numbers displayed in the table therefore give the rate in the number of atomic hops made in the time required to deposit one monolayer (i.e., the deposition time for L atoms). We have shown the rates for temperatures corresponding to our SOS-MBE results, as well as for those temperatures at which $R_n/R_D \sim 1$ for $n = 1-3$.

Dimension	T (K)	R_1/R_D	R_2/R_D	R_3/R_D	R_4/R_D	R_5/R_D
1	500	0.8	7.7×10^{-4}	7.2×10^{-7}		
	600	149	0.4	1.4×10^{-3}		
	650	1120	5.3	2.5×10^{-2}		
	700	6320	44	0.3		
2	500	1.6	1.5×10^{-3}	1.4×10^{-6}	1.4×10^{-9}	1.3×10^{-12}
	600	298	0.9	2.7×10^{-3}	8.2×10^{-6}	2.5×10^{-8}
	640	1530	6.6	2.9×10^{-2}	1.2×10^{-4}	5.4×10^{-7}
	700	12600	87	0.6	4.2×10^{-3}	2.9×10^{-5}

A particular surface atom's hopping rate is calculated from the Arrhenius expression $R_n = R_0 e^{-E_n/kT}$ where the prefactor $R_0 = d'kT/h$. The activation energy $E_n = E_0 + nE_b$ for an atom with n nearest neighbors and where E_b is the bond energy per neighbor; the exponential form of the rates leads to a great disparity in hopping rates between atoms in different bonding environments (see Table II). Our simulations are carried out in both 1+1 and 2+1 dimensions, and the parameters used are $E_0 = 1.0$ eV, $E_b = 0.3$ eV. The main difference between 1+1 and 2+1 dimensions manifests in the increased number of nearest neighbors available at higher dimensionality, leading to more effective relaxation for $d = 2 + 1$.

Since the deposition rate defines the time unit in our growth simulations (i.e., the average deposition rate is 1 layer/sec), the ratio of the atomic hopping rate to the deposition rate is the important dimensionless variable determining crossover behavior. In Table II, we give the numbers for this dimensionless ratio for our SOS-MBE simulations in $d' = 1, 2$ at various temperatures. Note that substantial crossover complications arise in the full SOS-MBE simulations (but *not* in the instantaneous-relaxation dynamical models) due to the existence of several different hopping rates. The existence of finite diffusion rates in the minimal MBE model leads to a competition between deposition and diffusion noise considerably complicating interpretation of simulational (and experimental) results.

C. Ballistic deposition model

This is the most complicated model (and numerically the most difficult to simulate) that we study, yet, as noted earlier, the most well understood asymptotically from the dynamic scaling standpoint. In Fig. 1(h), we illustrate in $d = 1 + 1$ the main difference between the BD and SOS models, namely, the existence of overhangs at the surface and voids in the bulk. For the purposes of defining the height function $h(\mathbf{x}, t)$, we simply choose $h(\mathbf{x}, t)$ to be the height coordinate of the highest occupied site above substrate position \mathbf{x} . While the multivalued character of ballistic aggregates may present certain problems in an analytical treatment, this definition of the height function has the advantage of being unique and does seem to be acceptable for studying scale invariant properties of the surface so defined.

In BD, the deposition rule is to select randomly a coordinate \mathbf{x} and the particle is added at the highest site above \mathbf{x} with an occupied nearest neighbor site. The relaxation rule also allows for holes or overhangs to be created: the hopping particle randomly selects a landing site from among the eight surrounding sites which are unoccupied and provide at least one nearest neighbor bond. No bias for upward versus downward hopping is made, and the hopping rates are exactly those used in the SOS model. We shall be concerned only with the stochastic-activated hopping version of this model since the basic BD model has been extensively studied in the literature in the context of KPZ universality [42]. A growth model intermediate between SOS and BD [20] models, where

the random deposition is SOS constrained but the activated hopping is BD constrained, has also been studied recently [38,43].

IV. RESULTS AND DISCUSSION

To put our results in context, we emphasize that Eq. (3.1) fixes the asymptotic form for the scaling function $g(y)$ exhibited by truly self-affine interfaces. In Fig. 2(a) (inset), we show the scaling collapse for the 3+ model [10] in $d = 2 + 1$ dimensions, and it clearly exhibits saturation for small y , and a power law increase for $y > 1$: this behavior can be seen in the superposi-

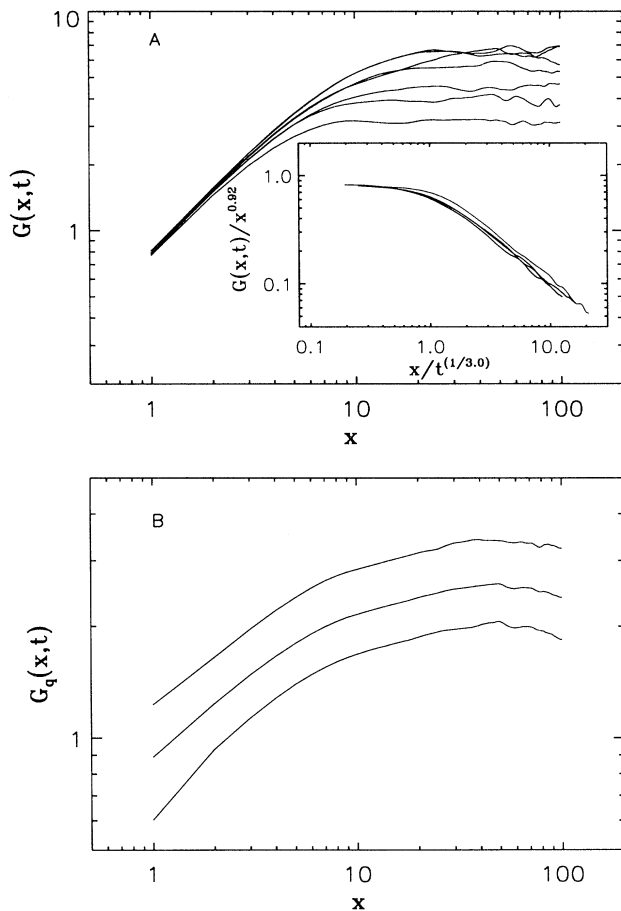


FIG. 2. (a) Correlation function $G(x, t)$ vs x for the 3+ model in $d = 3$ for times $t = 51, 109, 235, 505, 1084, 2324, 5000$ layers (bottom to top) and $L = 200$. Note the superposition of the various plots for small x . Inset: Scaling collapse $G(x, t)/x^{2\alpha}$ vs $x/t^{1/z}$ for $t = 109, 223, 504, 1083, 5000$ layers, with $2\alpha = 0.92$ and $z = 3.0$. (b) Plot of height-height correlation function $G_q(x, t)$ for the 3+ model in $d = 2 + 1$ for different moments $q = 1, 2, 4$ (bottom to top). From $x = 4$ to 10, $\alpha'_q = 0.32, 0.31, 0.31$ for $q = 1, 2, 4$, respectively. $L = 200, t = 5000$ layers.

tion of the data at small x in the uncollapsed $G(x, t)$ as shown in Fig. 2(a). Although the exponents here are not the asymptotic EW exponents [10] and these data are from a crossover regime, this model nevertheless demonstrates the typical behavior of the scaling function associated with self-affine surfaces. Furthermore, as shown in Fig. 2(b) by the parallel plots of G_1, G_2, G_4 (for $t = 1083$), this model's scaling function is independent of the moment q used in evaluating the height-height correlation function. This self-affine dynamic scaling behavior is by no means specific only to the 3+ model and is quite generic, holding for the 2+ and 4+ models [10], the Family model (see inset of Fig. 10 below), and the asymptotic BD model. In fact, this was the only known dynamic scaling behavior [42] in growth models until recent work [10–12,14] showed that MBE models may exhibit anomalous dynamic scaling. What we find in many of our MBE-inspired stochastic and dynamical growth models is that the scaling function $g(y = x/\xi)$ does not saturate at small y but shows an anomalous increase as $y^{-\kappa}$, and that the functions G_q yield q -dependent exponents, a signature of multiscaling behavior. Below we present observations on both types of models and speculate on their origins.

A. Anomalous scaling properties

The anomalous behavior of the scaling function has recently received much attention [10–15,35] in the context of DT-WV-type nonequilibrium models. Such models initially created interest because they suggested a continuum equation description for MBE growth dominated by fourth-order surface-diffusion terms, as in Eqs. (2.10) and (2.11), rather than the second-order surface tension (EW) term. Das Sarma *et al.* [11] have argued that the anomalous behavior of the scaling function is a reflection of the fact that the integral for the height-height correlation function $G(x, t)$ becomes divergent whenever the roughness exponent $\alpha \geq 1$, the so-called super-rough situation with $W(t \rightarrow \infty)/L$ diverging for $L \rightarrow \infty$. For example, a rather simple anomalous scaling behavior occurs in $d = 1 + 1$ [15] in the linear Mullins-Herring equation, Eq. (2.11), which is believed to apply exactly to the discrete LC model [13,14]. The system size L enters as an important cutoff in this super-rough situation, leading to the unexpected time dependence detectable in the correlation functions of anomalously scaling models. For super-rough models (where $\alpha \geq 1$), the behavior [11] of $G(x, t)$ is given by (with the correlation length $\xi \sim t^{1/z}$)

$$G(x, t) = \begin{cases} x^{2\alpha - \kappa} t^{\kappa/z}, & x \ll \xi \ll L \\ x^{2\alpha - \kappa} L^\kappa, & x \ll L \ll \xi \\ t^{2\beta}, & x \gg \xi. \end{cases} \quad (4.1)$$

For $x \ll \xi \ll L$, the quantity $G(x, t)/x^{2\alpha}$ does not saturate but scales as $y^{-\kappa}$ (where $y \equiv x/t^{1/z}$), precisely the anomalous behavior seen in both DT [11] and LC [13] models and in our more realistic stochastic Arrhenius hopping MBE growth models in both 1 + 1 and 2 + 1 dimension (see Figs. 3 and 4 below). In the regime where

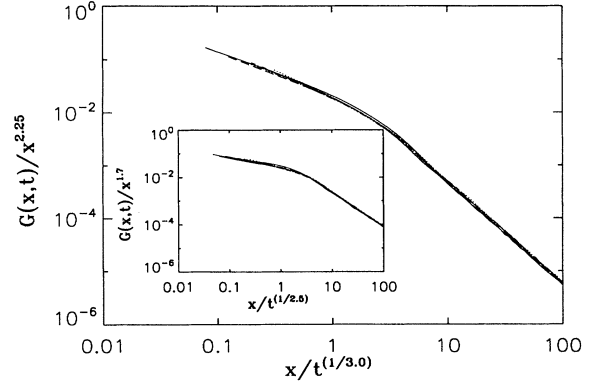


FIG. 3. Data collapse of the scaled height-height correlation function in $d = 1 + 1$ SOS-MBE for $T = 600$ K and $T = 650$ K (inset) with system size $L = 4000$ sites. Collapse is for seven times ranging from $t = 32$ to 2048; exponents are in Table III.

$\xi < L$ and the interface has not saturated, the anomalous scaling function corresponding to $g(y)$ in Eq. (3.1) is

$$G(x, t) = x^{2\alpha} \hat{g}(x/\xi), \quad (4.2)$$

where the anomalous scaling function $\hat{g}(y) = y^{-\kappa}$ for $y \ll 1$, and $\hat{g}(y) = y^{-2\alpha}$ in the large y limit. Whether the “exponent” κ which enters into Eqs. (4.1) and (4.2) is a true critical exponent, or rather a correction-to-scaling crossover exponent, is not a settled issue for all the models we study in this paper. For super-rough models with $\alpha \geq 1$, one must obviously have $\kappa \neq 0$ in a true sense because $G(x, t)$ for $x \ll \xi$ behaves as $x^{2\alpha'}$ where $\alpha' \leq 1$. The boundedness of the effective roughness exponent α' determining the short-distance behavior of the height-height correlation function follows very simply from a triangle inequality argument [44]. Thus, in situations where $\alpha \geq 1$, one must necessarily have

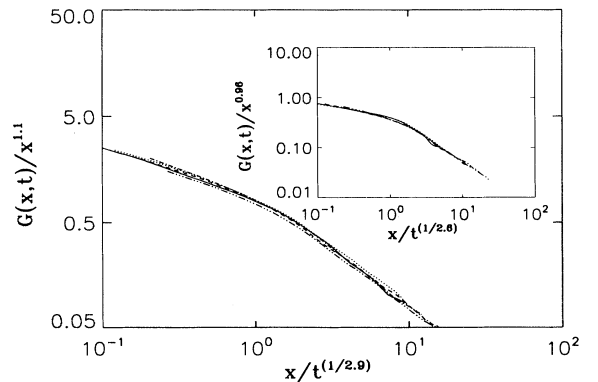


FIG. 4. Data collapse of the scaled height-height correlation function in $d = 2 + 1$ SOS-MBE for $T = 600$ K and $T = 640$ K (inset) with a system of $L = 500 \times 500$ sites. Collapse is for five times ranging from $t = 45$ to 1000; exponents are in Table III.

$\alpha' = (\alpha - \kappa/2) \leq 1$, making $\kappa \neq 0$ a *true* anomalous exponent. This is trivially demonstrated [11,15] by considering the height-height correlation function in the linear Eq. (2.11), whence one finds, in $d = 1 + 1$, that $\alpha = 1.5$ and $\alpha' = 1.0$, making $\kappa = 1$ for the ∇^4 linear model [45]. While the anomalous scaling behavior of all the linear super-rough models (i.e., ∇^{2n} -type models for $n \geq 2$) is trivially simple [45], the corresponding nonlinear situation has not yet been resolved theoretically [46]. Among the anomalously scaling discrete dynamical growth models, only the LC model [13], which exactly follows the linear Eq. (2.11), is completely understood so far. Particularly puzzling is the behavior of our Arrhenius-activated SOS-MBE growth models, which seem to exhibit anomalous dynamic scaling behavior ($\kappa \neq 0, \alpha' < \alpha$) somewhat weakly in $d = 2 + 1$ and very strongly in $d = 1 + 1$, independent of whether $\alpha \lesssim 1$. The anomalous scaling behavior even in the simple DT model is not yet completely understood [11,14,46]. One could attribute $\kappa \neq 0$ to an unusually long-lived transient in the $\alpha < 1$ situation, whose persistence over many decades in growth time (i.e., very slow crossover) is not yet theoretically understood. In the following we consider the nonzero value of κ in the scaling function found from our numerical simulations of a growth model as the operational signature of the existence of anomalous scaling in that particular growth model.

Figure 3 (4) shows the data collapse of the measured function $G(x, t)$ for 8 (5) values of t in $d = 1 + 1$ ($2 + 1$), presented as the observed scaling function $\hat{g}(y)$ versus $y = x/t^{1/z}$ for SOS-MBE models at two different temperatures. Excellent scaling collapses of the correlation function in both dimensions are obtained for both temperatures studied, and the exponent κ is nonzero, corresponding to the nonsaturation of the scaling function $\hat{g}(y)$ for small y . The scaling parameters κ, α, z are found to depend on the growth temperature (see Table III), and $\alpha \neq \alpha'$ because $\kappa \neq 0$. The values of α and z are estimated from the scaling collapse by changing z to provide the optimal fit using the constraint that $\beta (= \alpha/z)$ is the same as that extracted from $G(x \rightarrow \infty, t) \sim t^{2\beta}$. No extensive formal error analysis was performed; however, the displayed data collapses showed notable deterioration with changes of roughly ± 0.1 in 2α and $1/z$, which gives an approximate upper bound on the *statistical* errors involved. Clearly the scaling function $g(y)$ for a self-affine interface cannot explain these observations—the inset of

Fig. 2 shows a saturation in the normal scaling function not observed here even for very small y . We emphasize that the possibility of saturation of $\hat{g}(y)$ for substantially smaller values of y than investigated in our simulations obviously cannot be ruled out (i.e., κ may eventually vanish for very long times), but nevertheless the observed anomalous behavior is intriguing.

Additionally, we directly compare the function $G(x, t)$ in $d = 1 + 1$ for SOS and BD Arrhenius hopping models at $T = 600$ K for identical activation parameters. The anomalous time dependence of $G(x, t)$ in Eq. (4.1) can be easily seen for the SOS model in Fig. 5(a) as $G(x = 1, t)$ does not saturate ($\kappa \neq 0$), while in the BD model [Fig. 5(b)] the values of $G(1, t)$ quickly attain a saturated value implying $\kappa = 0$. The SOS 3+ model shares the behavior of the BD model [Fig. 2(a)]; however, there the saturation occurs much earlier in time. In Fig. 5(c) we show explicitly the continued growth of average step height, $G(1, t)$, in the SOS-MBE model for $T = 600$ and 650 K, a striking contrast to the situation in the $T = 600$ K BD MBE model (top line), which after a transient for $t \leq 100$ layers shows $G(1, t)$ saturating consistent with the asymptotic self-affine scaling associated with the KPZ equation. The continued increase of $G(1, t)$ in the minimal SOS-MBE model out to extremely long times is the most dramatic manifestation of anomalous scaling in such models, and while it could be a transient behavior, the associated crossover time is evidently exceedingly large.

The asymptotic scaling parameters for BD at $T = 600$ K calculated at late times, $z = 1.5$ and $\alpha = 0.45$ as obtained from the scaling collapse in Fig. 6, are indeed consistent with those of the KPZ equation for $d = 1 + 1$ [47]. Interestingly, the early time growth in the BD model shown in the inset of Fig. 6 appears consistent with other Arrhenius studies of BD [19,22,37], exhibiting an SOS-like transient detected in the collapse by the markedly larger values of $z = 2.7$ and $\alpha = 1.0$ for earlier times than the asymptotic KPZ values. (Although the scaling collapse does not saturate in the inset of Fig. 6, the extent is too small to definitively conclude that this time regime in BD shows anomalous scaling on these grounds.) As the BD growth model crosses over to the asymptotic KPZ scaling (initiated by defect nucleation [22]), the time dependence vanishes as shown in Fig. 5(b). The existence of the strong early time SOS transient explains why $G(1, t)$ does not saturate until fairly late in the simulation for

TABLE III. Collection of scaling parameters calculated from the scaling collapses in Figs. 3 and 4 using the relations $2\alpha = 2\alpha' + \kappa$ and $z = z'/(1 - \lambda)$ with $\kappa = \lambda z$. We define $\beta' = \alpha'/z'$. The quantity $z_1 = \alpha'/\beta$ is an artificial “exponent” constructed from incompatible exponents which give a much lower value than $z = \alpha/\beta$.

Dimension	T (K)	α	β	z	κ	λ	α'	β'	z'	z_1
1	600	1.12	0.37	3.00	0.96	0.32	0.64	0.31	2.04	1.73
1	650	0.85	0.34	2.50	0.47	0.19	0.61	0.30	2.03	1.79
2	600	0.55	0.19	2.90	0.49	0.17	0.31	0.128	2.42	1.63
2	640	0.48	0.184	2.60	0.26	0.10	0.34	0.146	2.33	1.84

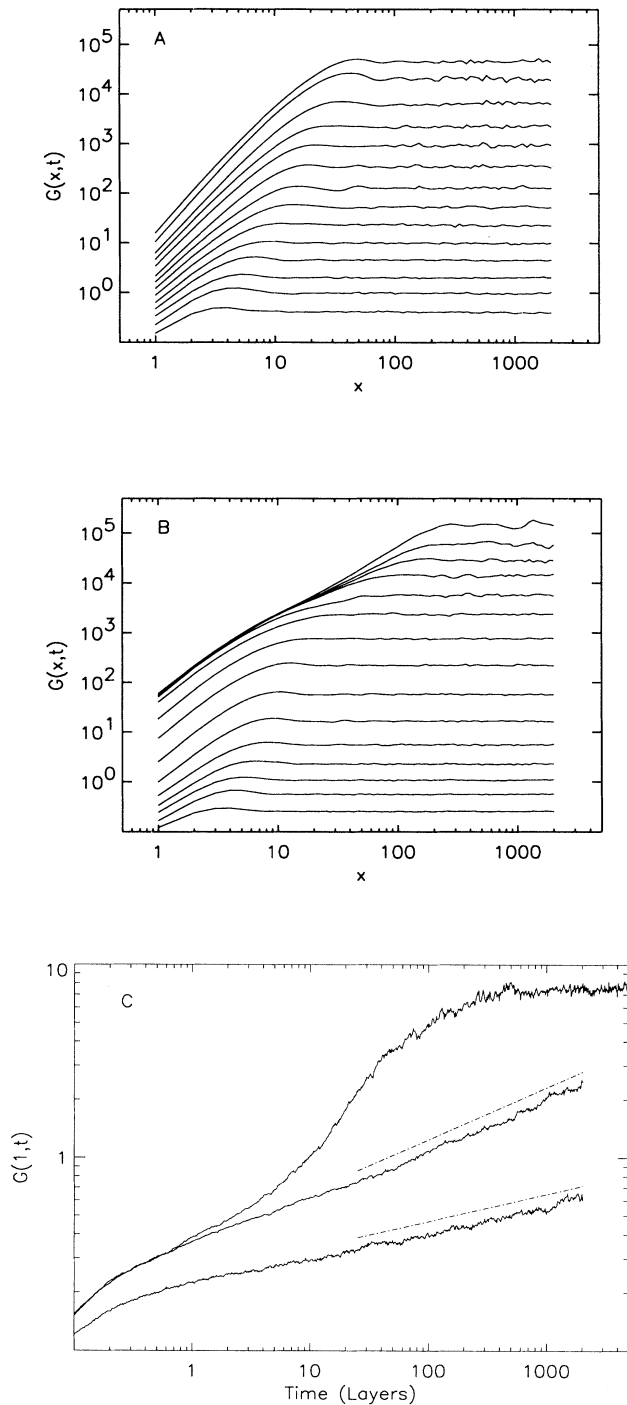


FIG. 5. Raw correlation function vs distance x for times $t = 2^j, j = -2, -1, \dots, 11, 12$ in the SOS-MBE model (a) and BD model (b) at $T = 600$ K in $d = 1 + 1$ ($L = 4000$). Note the different behavior for small x as a function of time; compare these as well with Fig. 2(a) for the 3+ model. (c) $G(1,t)$, or equivalently, the mean square slope of the interface, versus time for BD (top) and SOS at $T = 600$ K (middle), and SOS at $T = 650$ K (bottom). The slopes equal to κ/z of the dashed lines are 0.27 ± 0.02 and 0.14 ± 0.02 for the $T = 600$ and 650 K SOS cases, respectively. (Compare with $\kappa/z_{600} = 0.32$ and $\kappa/z_{650} = 0.19$ from Table IV.)

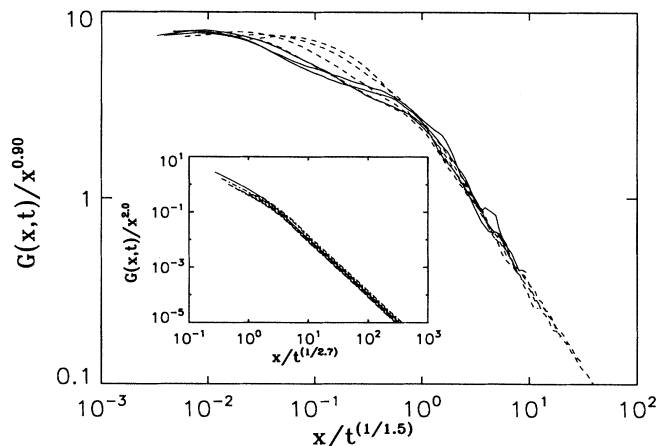


FIG. 6. Data collapse of the late time behavior of the correlation function in the BD model at $T = 600$ K with $L = 4000$, for six times ranging from $t = 128$ to 4096 : $2\alpha = 0.90, z = 1.5$. The inset shows data from the same simulation, at seven times from $t = 0.5$ to 64 , but now $2\alpha = 2.0$ and $z = 2.7$, consistent with the idea of a SOS transient in the BD model.

BD as compared to the 3+ model (Fig. 2). Our activated hopping finite temperature MBE growth simulations involving SOS deposition and BD diffusion rules (not presented here) show even stronger and longer lasting SOS transients, consistent with other findings in the literature [19,37,38,43].

Figures 2–6 demonstrate that the qualitative features of the scaling function depend upon the microscopic local discrete growth rules. In fact, we point out that the phenomenology suggested by our results is that models (3+, BD, etc.) which are asymptotically described by a second-order continuum equation (EW or KPZ) have $\kappa = 0$ while those models (SOS MBE, DT, LDS, LC, WV, etc.) which are thought to be dominated (at presently accessible simulational time scales) by fourth-order chemical bonding-driven diffusion terms, $\nabla^4 h, \nabla^2(\nabla h)^2$, etc., tend to give anomalous scaling with $\kappa \neq 0$. In a more practical vein, the behavior of our stochastic SOS-MBE model suggests that in real MBE growth different experimental conditions may lead to different sets of observed exponents [e.g., one may be measuring the correlation function exponent $\alpha' = \alpha - \kappa/2$ from Eq. (4.1) and not the roughness exponent α characterizing the scaling behavior of the width]. The nonsaturation of $\hat{g}(y)$ at small y , in particular, suggests that there is the possibility of another (nontrivially large) time or length scale in the growth scenario as has been observed in the case of DT and WV models [11,12].

Schroeder *et al.*, [12] have analyzed in detail the anomalous time dependence of the height-height correlation function in the WV model, which is now believed [16,35] to eventually cross over to EW universality even though there is an extremely long initial transient where $\kappa \neq 0$. The WV model behaves almost the same as the

more nontrivial DT model in the long transient regime. Motivated by the time dependence in the average step height, $G(1, t) \sim t^\lambda$, with $\lambda = \kappa/z$, and considering it to define characteristic length and time scales, they have rewritten the scaling of the correlation function as

$$G(x, t) \sim x^{2\alpha'} t^\lambda g(x/\xi'(t)), \quad (4.3)$$

where $\xi'(t) \sim (t/t^\lambda)^{1/z'} = t^{(1-\lambda)/z'}$, as distinct from $\xi(t) \sim t^{1/z}$. The unit of time $t_s(t) \equiv t^\lambda$ adopted in Eq. (4.3) has been taken as a characteristic time associated with the growth of the average step height [12], $G(1, t)$. Therefore in reduced time units the effective correlation length $\xi' = t_r^{1/z'} \equiv (t/t_s)^{1/z'}$ parametrizes, through the exponent z' , the dynamical spread of correlations in terms of a *reduced* time t_r which is the physical time t measured in units of the changing scale $t_s(t)$. The exponent z , on the other hand, simply quantifies how the growth of the correlation length $\xi(t)$ scales with the physical time t . The descriptions in Eqs. (4.1) and (4.3) are completely equivalent descriptions of anomalous dynamic scaling at small x provided that $\kappa = \lambda z$, and α' is in fact exactly the exponent obtained from the small x behavior of $G(x, t)$ in Eq. (4.1). The relationship between these exponents [12] and the ones [11] appearing in Eq. (4.1) is given by $2\alpha = 2\alpha' + \kappa$ and $z = z'/(1 - \lambda)$, and (α, α') and (z, z') are numerically different whenever κ (or λ) is nonzero (i.e., in the presence of anomalous dynamic scaling).

The calculated scaling parameters $\alpha, \alpha', z, z', \kappa$, and λ as obtained from our simulations are collected in Table III for our SOS models in $d = 1 + 1$ and $2 + 1$: the anomalous exponent $\kappa = \lambda z \neq 0$ is obtained from the slope of the small y region of Figs. 3 and 4. We note that α, z , and κ all vary with temperature due to the usual finite size effects, and hence any experimental MBE growth exponent obtained by measuring width as a function of system size is expected to have temperature dependence. However, notice in Table III that the parameters α' and z' are not significantly sensitive to changes in temperature and are nearly constant, although their values do not correspond to any known universality class as defined by the continuum growth equations (Table I). The relevance of this observation is not clear since the SOS-MBE model may be in a transient regime for these particular simu-

lations, but it is interesting to note that several $(1 + 1)$ -dimensional nonequilibrium dynamical models also have $\alpha' \sim 0.63$ (Table IV), as presented below. As emphasized before, an interesting and possibly important point is that $\alpha < 1$ in all cases but one in Table III: this demonstrates that anomalous dynamic scaling according to Eq. (4.1) is not merely an artifact of a trivial growth instability associated with super-roughening (i.e., $\alpha \geq 1$). While super-roughening ($\alpha \geq 1$) is certainly a sufficient condition for anomalous scaling, at this stage it does not appear to be a necessary condition.

We find that the exponent $2\alpha'$ calculated directly from $[\partial \ln G(x, t)/\partial \ln x]$ in the limit of small x increases with time, saturating at late times [$\sim L$ layers in $d = 1 + 1$ when $\xi(t) \gg x$]. For $T = 600$ K, we have confirmed that α' has saturated at the latest times in the simulation, whereas for $T = 650$ K, a slight increase in α' can still be observed: our $d = 2 + 1$ results both show saturation of α' . This gives us a consistency check on the value of α' found in the anomalous scaling situation from the scaling collapses and both methods of obtaining α' gave equivalent numerical results. Nevertheless, we cannot rule out that transients are influencing the interfacial dynamics such that it scales in a nonuniversal manner. Further, the very large time scales over which such crossover effects operate are physically relevant, and seem likely to show up in experiments. Its complete understanding remains a serious issue in terms of interpreting experimental results which may reside in this regime, and may considerably complicate experimentally extracted roughness exponents.

In conservative models which obey the SOS restriction one expects the hyperscaling relations $z = 2\alpha + d'$ and $z' = 2\alpha' + d'$ to hold [8,12]. From the data in Table III for our minimal MBE model, we find agreement at the 5 – 10% level with both forms of the hyperscaling relation for $d' = 1$ and 2 [although the values of $2\alpha + d'$ ($2\alpha' + d'$) are consistently high as compared to the measured values of $z(z')$]. Additionally, from the definition of the structure factor, one has the relation $2\alpha' + d' = \gamma$, where the structure factor scales as $S(k) \sim k^{-\gamma}$ in the saturation regime $t \rightarrow \infty$, or equivalently, $\xi > L$, so that $\gamma = z'$ (the dynamical exponent describing the spread of correlations in reduced time t_r) due to the hyperscaling relation. We show in Fig. 7 plots of $S(k)$ for $d = 1 + 1$ and $2 + 1$ at $T = 600$ K for various small system sizes L . In both cases, we have observed a systematic increase of γ with L , and for the largest systems we find $\gamma = 2.60 \pm 0.05$ ($L = 200$) and $\gamma = 2.55 \pm 0.10$ ($L = 40$) in $d = 1 + 1$ and $2 + 1$, respectively (results for still larger L indicate that there is little further increase in γ). Our $d = 2 + 1$ result for γ agrees within the error bars with the value $z' = 2.42 \pm 0.15$ extracted from the simulations, and the observed value $2\alpha' + d' = 2.6 \pm 0.1$. However, in two dimensions we find from our simulations that while $\gamma = 2\alpha' + d' \sim 2.3$ and the hyperscaling relation $z' = 2\alpha' + d'$ each hold at $\approx 10\%$ level, $\gamma = 2.6$ and $z' = 2.0 \pm 0.2$ are very different for reasons that are not clear, but likely are related to finite size and time effects [48]. Except for this discrepancy [48], the various hyperscaling relations are seen to hold for our realistic

TABLE IV. Collection of scaling parameters from the scaling collapses of Fig. 8 for the Family, LDS, DT, and TDH dynamical models in $d = 1 + 1$. In all cases, the system size is $L = 10\,000$ and $t_{\max} = 10\,000$, and $\alpha' = \alpha - \kappa/2$ is surprisingly constant for LDS, DT, TDH.

Exponent	Family	LDS	DT ($D=1$)	TDH
α	0.50	1.03	1.40	1.54
β	0.25	0.34	0.37	0.38
z	2.0	3.04	3.74	4.03
κ	0.06	0.75	1.56	1.85
α'	0.47	0.65	0.62	0.61

MBE model.

In order to develop a better understanding of our minimal SOS-MBE simulations, we now display the scaling collapse of the Family [Fig. 8(a)], LDS [Fig. 8(b)], DT, and TDH [Fig. 8(c)] model results, and in Fig. 9(a) compare the interfacial morphology for these models. The Family model is the only model in Fig. 8 which shows explicitly the rapid saturation of $g(y = x/t^{1/z})$ for $y \ll 1$ expected for a growing self-affine interface [Eq. (3.1)]. Our numerical scaling collapse data for surface-diffusion-driven LDS, DT, and TDH models show the continued increase in $\hat{g}(y)$ for $y < 1$ in marked contrast with the purely self-affine dynamic scaling behavior of Eq. (3.1), but in complete agreement with the anomalous scaling behavior defined in Eqs. (4.1) and (4.3). In fact, the scaling collapse for the DT, LDS, and TDH models shown in Fig. 8 is very similar to the corresponding SOS-MBE

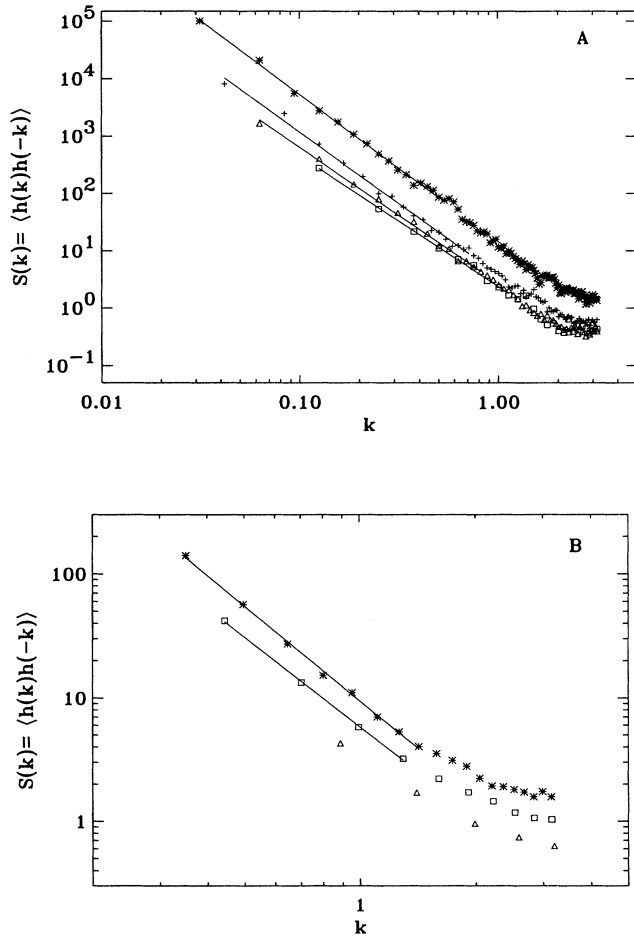


FIG. 7. Plot of the structure factor $S(k)$ at $T = 600$ K for various system sizes for SOS-MBE in (A) $1 + 1$ and (B) $2 + 1$. The system sizes in $d = 1 + 1$ are $L = 50$ (\square), 100 (\triangle), 150 ($+$), 200 ($*$), and for $d = 2 + 1$, $L = 10$ (\triangle), 20 (\square), 40 ($*$). Slopes for the largest systems are 2.6 ± 0.05 and 2.55 ± 0.10 in $d = 1 + 1, 2 + 1$, respectively.

scaling collapse shown earlier (cf. Figs. 3 and 4), reinforcing our claim that the qualitative aspects of anomalous dynamic scaling in real SOS-MBE growth are captured in the instantaneous-relaxation nonequilibrium growth

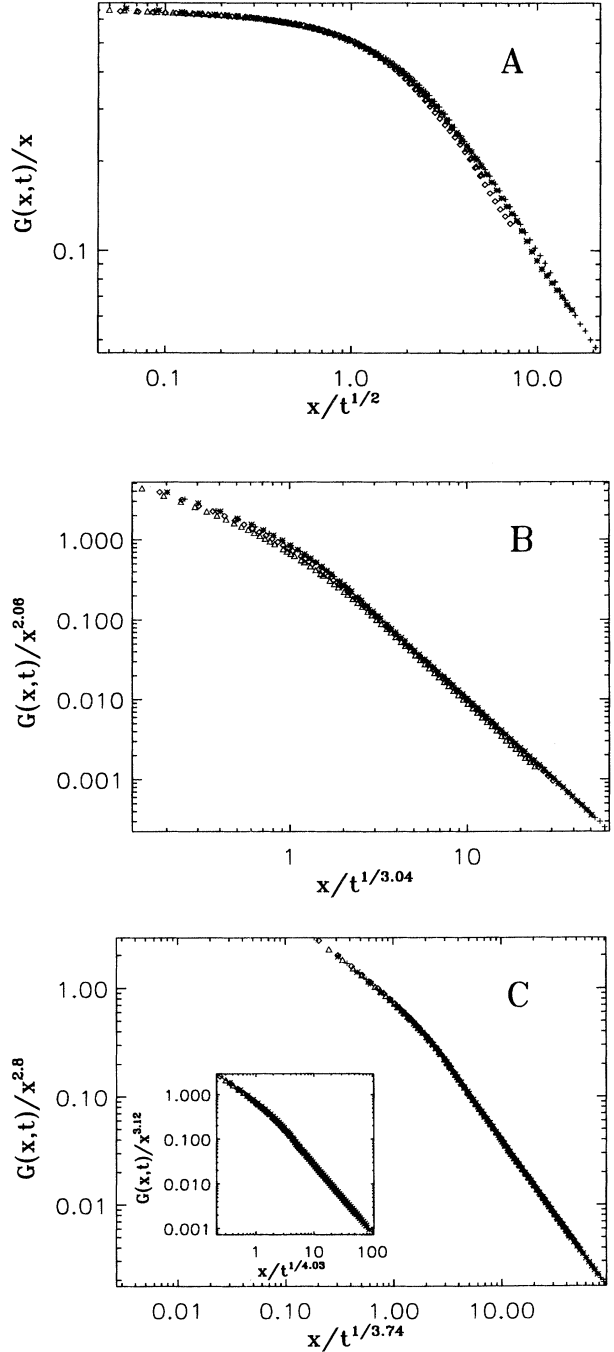


FIG. 8. Scaling collapses displaying $G(x,t)/x^{2\alpha}$ vs $y = x/t^{1/z}$ for various dynamical models for $t = 524, 1060, 2100, 4900, 10000$ for a system size of $L = 10^4$: (a) Family, (b) LDS, and (c) DT (TDH in inset). Notice how only the Family model saturates at small y , all other models are increasing for decreasing y .

models of DT type.

Notice first in Fig. 9 the great difference in the vertical scale in the morphologies of the four dynamical models, and how the DT model in particular generates very sharp, deep grooves, but otherwise shows little short-wavelength kinetic roughness. The line below each morphology in Fig. 9 shows the spatial step-height distribution by plotting the step size as a function of position: while the Family model's distribution of steps across the system appears simply noisy (ostensibly with a Gaussian probability distribution), the other models demonstrate occasional very large steps above the background step size, and thus exhibit very violent "intermittent" fluctuations. Also in Fig. 9 we show representative saturated SOS-MBE growth morphologies at two different temperatures with the corresponding spatial distributions of step heights shown at the bottom of each morphology. A visual comparison manifestly establishes the similarity between the SOS-MBE morphology and that in the DT (or, for that matter, LDS or TDH) model with the SOS-MBE

step-height distribution exhibiting violent "intermittent" fluctuations similar to those shown in Fig. 9 for the DT model. It is also obvious that the Family model results are qualitatively different from the SOS-MBE results.

These qualitative considerations are further strengthened by actually calculating the exponents α, z, κ , etc. corresponding to Fig. 8 for the dynamical discrete models which are collected in Table IV. We note that the set of exponents α, β, z in each case (ignoring TDH for the moment as we expect it to be severely limited by finite size effects) is quite consistent with that of a standard continuum equation description: Eq. (2.5) for the Family model, Eq. (2.10) for LDS, and Eq. (2.11) for the DT model. Only the Family model exhibits the usual self-affine dynamic scaling ($\kappa = 0$) consistent with the continuum EW description of Eq. (2.5). But, the calculated anomalous exponent $\kappa \approx 1.56 \pm 0.06$ for the DT model is significantly larger than the value of 1.0 expected on the basis of linear Eq. (2.11). Thus the linear fourth-order Herring-Mullins equation, Eq. (2.11), cannot be a

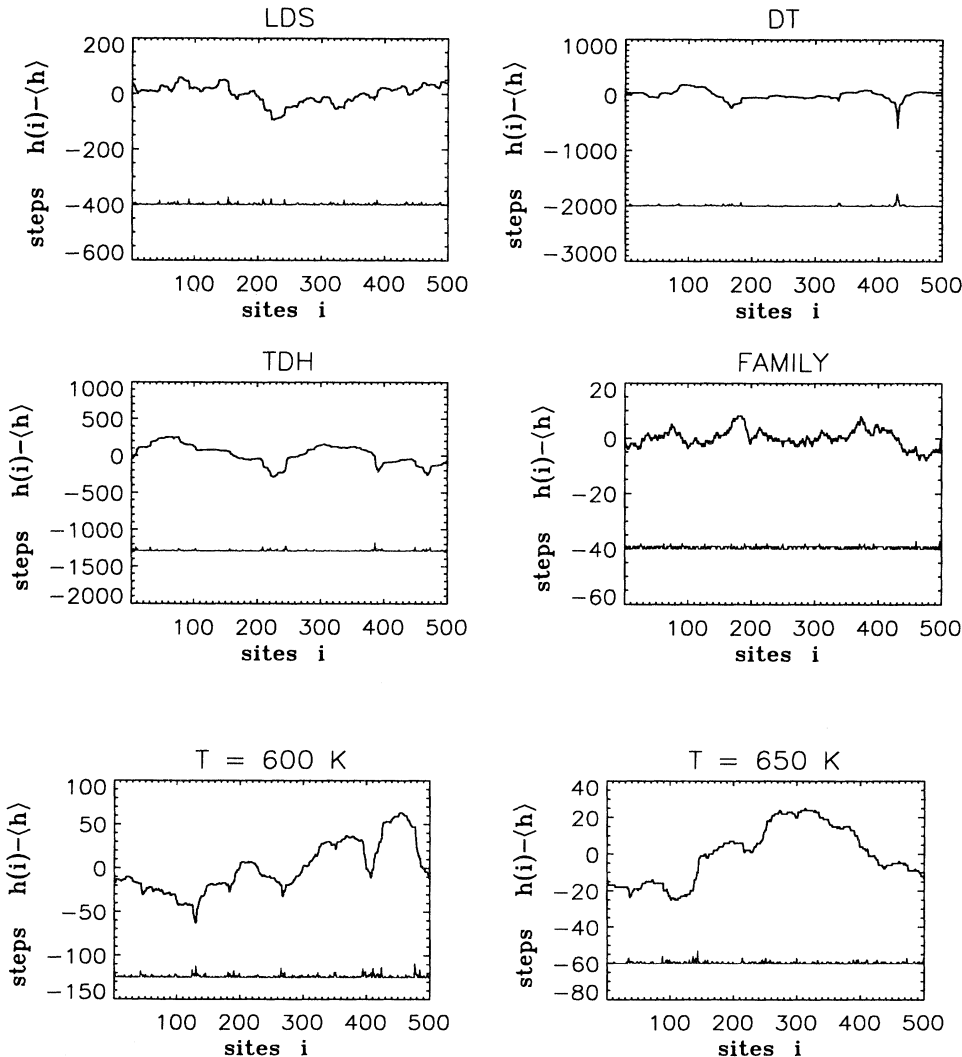


FIG. 9. Morphologies of several dynamical models for $L = 500$: LDS model for $t = 1 \times 10^5$ layers; DT model for $t = 1 \times 10^6$ layers; TDH model after $t = 1 \times 10^6$; Family model at $t = 1 \times 10^6$. The lower plot in each figure shows a trace of the step height at each site. Note the very different vertical scale in the various cases as dictated by the widely changing scaling exponents. We also show saturated ($t = 131072$ layers) SOS-MBE morphologies for $T = 600$ and 650 K in $1+1$ dimensions for $L = 500$. We include the step-height distributions for comparison of the intermittent properties of the two classes of models.

complete description for the discrete DT model, a point recently emphasized in the literature [10,11,13,14]. In the LDS model, we find $\kappa = 0.75 \pm 0.05$, but the non-linearity of Eq. (2.10) does not allow for an analytical comparison [46] for the value of κ . If one naively assumes that $\kappa = 0^+$ for Eq. (2.10) in $d = 1 + 1$ based on the fact that $\alpha = 1$, then one concludes again that κ for the discrete LDS model is substantially larger than that for Eq. (2.10). The TDH model, with its added time-delayed hopping of certain atoms, shows slightly rougher growth both in time and space than the DT model, and also seems inconsistent with Eq. (2.11) due to the large value of $\kappa \approx 1.85$. Surprisingly, though, we find that $\alpha' = 0.63 \pm 0.02$ for the DT, LDS, and TDH models, essentially the same value as in the corresponding minimal MBE model in $d = 1 + 1$. At least for this temperature and time regime, then, the instantaneous-relaxation dynamical models do capture certain quantitative aspects of the minimal MBE growth model.

Next, we discuss a possible mechanism giving rise to anomalous dynamical scaling in these models. The anomalous aspect of the scaling behavior is associated with the time dependence of $G(x, t)$ for small values of x . Such a time dependence for $G(1, t)$ (the root-mean-square step-height fluctuation at time t) means that statistically the height fluctuations between any two neighboring columns is increasing in time. But certainly, the typical step height must be bounded from above by the interface width. To keep the step-height fluctuations from growing to the size of the width, there must then be net local downward transfer of particles in response to nearby height fluctuations. We illustrate the importance of such responsive downward hops using the Family model, which explicitly forces downward hops in response to height fluctuations, modifying it to reduce the response. Our modification of the Family model for this purpose consists of introducing an effective barrier to hopping down to the local height minimum, characterized by a parameter $p \in [0, 1]$, where p is the probability that the chosen down hopping process to the local height minima will occur. The original Family model corresponds to $p = 1$ whereas $p = 0$ is growth by pure random deposition. Figure 10 shows the scaling collapse of $G(x, t)$ for two cases, $p = 1.0$ and 0.05 . The introduction of the barrier does induce a time dependence in $G(x, t)$ for small values of x , leading to a transient anomalous dynamic scaling behavior with effective $\kappa \neq 0$ in the crossover regime prior to when EW behavior eventually sets in. This confirms the idea that a reduction in the local downward hopping can cause anomalous time dependence akin to that in Eq. (4.1). Ultimately, however, at a crossover time depending upon the specific value of p (with lower p leading to longer crossover time scales), saturation of the scaling function occurs in this modified Family model for all p studied, suggesting that anomalous scaling for this model at least is purely a crossover phenomenon.

In our activated Arrhenius MBE growth model, while there is no explicit barrier to down hops, neither is there an explicit driving force to lower heights [e.g., consider atoms a, b, c, e in Fig. 1(g)]. Atoms which hop choose their landing sites randomly, causing an effective reduc-

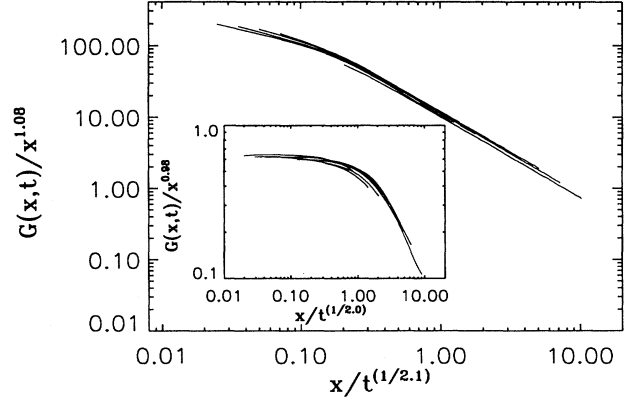


FIG. 10. Scaling collapse for the modified Family model with $p = 0.05$ at $t = 120, 251, 524, 1096, 2290, 4786, 10\,000$ for $L = 200$: $z = 2.1$, $\alpha = 0.54$, $\beta = 0.26$. Note the lack of saturation of the collapse. In the inset, the unmodified Family model is shown ($p = 1.0$), and the scaling function quickly saturates. Same times and size used, and $z = 2.0$, $\alpha = 0.49$, $\beta = 0.245$.

tion in the downward mobility compared with that in the Family model. Since growth rules that allow hopping in response just to the nearest neighbor height fluctuations show EW universality [i.e., normal dynamical scaling with asymptotic behavior given by Eq. (2.5)], one expects net downward hopping of sufficient strength may also generate such a term. We cannot precisely define “sufficient,” but the modified Family model with $p = 0.05$ clearly shows that transient effects not normally present can enter when the strength of downward hopping is suppressed even while the asymptotic scaling has EW character. Depending on the growth rules, however, the corresponding $\nu_2 \nabla^2 h$ term can be nearly vanishing (as appears to be the case for the WV model [16,35]), or in cases such as the LC model, where $\nu_2 \equiv 0$ and the $\nabla^2 h$ term vanishes exactly [13,14] in spite of considerable downward motion [Fig. 1(f)]. These observations indicate that anomalous scaling may be subtly related to the underlying microscopic growth rules which dictate how atoms seek out stable sites. It is also obvious from these considerations that there are at least two possible different scenarios producing $\kappa \neq 0$ (i.e., anomalous dynamic scaling), namely, the mechanism of suppressed downward hopping which is effective in our modified Family model (and, presumably in the WV model) where κ is purely a crossover exponent, and the mechanism effective in the LC model (which is related to super-roughness) where κ is exactly unity and is not a pure crossover effect phenomenon. The discrete DT model, which is the most relevant dynamical model underlying the minimal SOS-MBE growth model, is suggested to have $\nu_2 = 0$ based on symmetry arguments [41], and therefore the anomalous dynamic scaling in the DT model (and, presumably in LDS and TDH, and by inference, in the minimal MBE growth model) could be expected to be an intrinsic phenomenon (at least in $d = 1 + 1$) and not a crossover

effect. (It is possible, however, that the observed anomalous dynamic scaling in SOS-MBE growth in $d = 2 + 1$ is a crossover effect related to suppressed downward hopping.)

Dynamical models exist in which particle diffusion does not respond to the height difference between two sites, but to another local geometrical property, such as the LC model wherein diffusion is explicitly driven by the curvature of the local interface. Particle transfer between the neighboring sites therefore is not exclusively determined by the nearest neighbor height fluctuations, but includes the effects of more remote sites. Of course, there are situations in which the particles do hop downwards in the LC model in response to the curvature [atoms a , f , Fig. 1(f)]. However, they are only implicitly responding to the nearest neighbor height fluctuations, while the unifying characteristic driving all diffusion is the curvature. The LC growth rules limit the number of downward hops that decrease the height (atom c), and in some cases permit hopping to increase the height (atoms b , e). Note that in $1+1$ dimensions the curvature measured at a kink site is always greater than that at the top edge of a cliff or at a flat terrace site, so an in-plane hop to a kink site (atom c) or an upward hop to a kink site (atom b) is *only* dictated by the curvature difference.

A similar analysis of Fig. 1(c) for the DT model shows that various processes can (and cannot) occur when driven by the microscopic rule of increasing the local bonding: hopping to lower sites (atoms a , c , f), curvature-driven hopping (atom c), the *lack* of hopping to lower sites (atom e), and the *lack* of curvature-driven hopping (atoms b , e). The DT model (together with the WV and stochastic SOS-MBE models) in some sense is then “impure.” While the Family and LC models allow diffusion consistent with a single geometrical rule (height- or curvature-driven relaxation, respectively) and produce scaling consistent with a single linear continuum equation [Eq. (2.5) and (2.11), respectively], the DT model has subsets of processes which belong to both height-driven and curvature-driven geometrical rules, and certain processes consistent with neither [atom e in Fig. 1(c) does not move; cf. Figs. 1(a) and 1(f)]. Hence the DT (and SOS-MBE) results are close to but not exactly those of the LC model: Eq. (2.11) predicts $\kappa = 1.0$, and the LC model shows $\kappa \sim 0.96$ [13], while for the DT model the nearest neighbor height fluctuations are stronger, with $\kappa = 1.6$ (see Table III and Ref. [11]). Our qualitative geometric discussion here is based entirely on linear growth equations, Eqs. (2.5) and (2.11), because it is easy to identify geometric rules which correspond to linear growth terms. The DT interface morphology (as well as that for the minimal MBE model) very clearly indicates that any underlying continuum description (if it exists) must necessarily be nonlinear for these models (see also the discussion below on the lack of up-down symmetry), and the relevance of this qualitative geometric discussion to the DT (and the SOS-MBE) model remains questionable.

In the above discussion we have noted a connection between a strong tendency of atoms to move downward to self-affine scaling behavior (Family, $3+$, BD), while

inhibition of downward motion (DT, LC, Family with $p < 1$) leads to anomalies in the scaling function. Since the SOS-MBE model, by allowing atoms to hop to any site independent of final coordination numbers and height differences, inhibits local downward mobility, it is qualitatively (and for α' , quantitatively) similar to the dynamics of the DT model. Of course, how strong the downward motion must be to avoid anomalous scaling remains unclear, but the decrease in the value of κ (Table III) with increasing temperature is understandable, considering that the higher bond cutting processes are activated at higher temperatures and global height minima are more easily reached through multiple hops of a single atom. But, at higher temperatures, diffusion lengths are enhanced exponentially [28] making the (conserved) diffusion noise η_D dominant over fairly large distances, leading to smooth layer-by-layer growth, and the whole issue of deposition noise-induced kinetic roughening becomes essentially moot.

B. Multifractality and up-down symmetry breaking

Recently the DT model has been studied by Krug [14] as an example of multifractality [39] with the phenomenology of the DT model showing striking similarities to fluid turbulence intermittency [40,49]. We have applied Krug’s analysis to our minimal MBE growth model and to a number of dynamical growth models. A multifractal interface can qualitatively be thought of as the union of several self-affine fractal surfaces possessing a range of exponents. One of the signatures of multifractal behavior, as distinct from simple self-affine surfaces, is q -dependent exponents, where the integer q denotes the q th moment of the height fluctuations as in Eq. (3.2). For the special case of a self-affine surface, all the α'_q are equal. The step-size distribution function $P(s)$ of a multifractal surface is a stretched exponential with $\delta < 2$, not the Gaussian shape ($\delta = 2$) of a simple self-affine interface. Below we discuss our results on the multifractality of the stochastic SOS-MBE model and of various dynamical models separately. We also discuss the associated issues of the $h \rightarrow -h$ symmetry breaking in the evolving interface morphology and of the intermittency phenomenon in the step-height distributions.

1. Stochastic models

In Fig. 11, we show $G_q(x, t)$ for $q = 1, 2, 4, 6$ for $d = 1 + 1$ ($q = 1, 2, 4$ for $d = 2 + 1$ —inset) at $T = 600$ K at the longest times of our simulations. The multifractal behavior is evident from these plots based on the inequality of the initial slopes of the various curves, defined as $\alpha'_q = \partial \ln G_q(x, t) / \partial \ln x$. Note that α'_2 is precisely $\alpha' = \alpha - \kappa/2$, and that α'_q is a monotonically decreasing function of q , from 0.84 ($q = 1$) to 0.41 ($q = 6$) in $1 + 1$ dimensions, and 0.34 ($q = 1$) to 0.20 ($q = 4$) for $d = 2 + 1$.

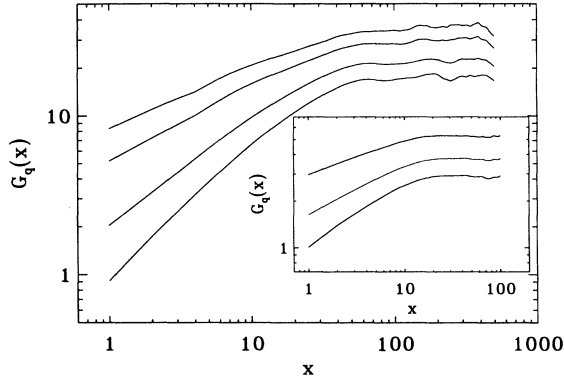


FIG. 11. Multi-affine behavior of the correlation function $G_q(x,t)$ for the SOS-MBE models in $1+1$ dimensions, $T = 600$ K, $L = 1000$ after 8192 layers grown. The moments $q = 1, 2, 4, 6$ are displayed (from bottom). Inset: $2+1$ dimensions, $T = 600$ K, $L = 500$ after 1000 layers grown. The moments $q = 1, 2, 4$ are shown from bottom to top. The variation in initial slope here indicates multi-affinity.

In the DT model [14], in addition to the q -dependent exponents for higher moments, the $h \rightarrow -h$ symmetry of the interface is manifestly broken as evidenced by sharp pits being carved out of the bulk without any equally sharp peaks [Fig. 9]: clearly the inverted interface has a very different morphology. This is also true in our $d = 1+1$ SOS-MBE growth results where the $h \rightarrow -h$ symmetry is also manifestly broken, as shown earlier in Fig. 9. In Fig. 12, the nonsaturated morphologies of our $d = 1+1$ Arrhenius-activated hopping model at $T = 600$ K are shown in more detail and indeed the $h \rightarrow -h$ symmetry is clearly absent. The breaking of $h \rightarrow -h$ symmetry implies only the existence of nonlinear nonequilibrium terms in the growth equation which manifestly violate detailed balance, and must therefore vanish in the limit of zero incident flux. Figure 13 shows a typical morphol-

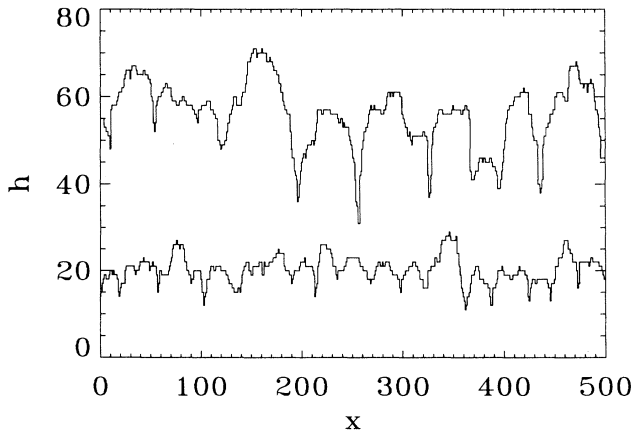


FIG. 12. Morphology of the SOS-MBE surface at $t = 100, 4000$ monolayers at $T = 600$ K, $L = 4000$.

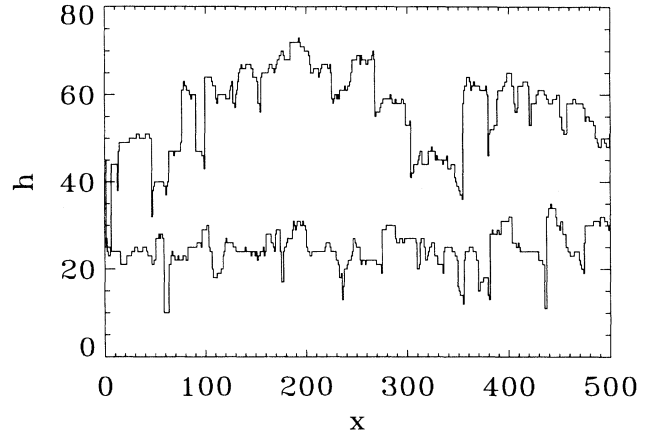


FIG. 13. Morphology of the BD surface at $t = 100, 4000$ monolayers at $T = 600$ K, $L = 4000$.

ogy for the BD model, showing the expected asymmetry due to the nonlinear KPZ term $(\nabla h)^2$ which manifestly breaks the $h \rightarrow -h$ symmetry. However, no multi-affine behavior is present in the BD results and neither is there asymptotic anomalous scaling behavior [Figs. 5(b), 6]. Based on this we conclude that asymmetry in the surface morphology is not a sufficient condition for the existence of multi-affine behavior, but is necessary. The only concrete, definitive implication of $h \rightarrow -h$ symmetry breaking is that any underlying continuum equation must necessarily be nonlinear and nonequilibrium, establishing that the linear Eq. (2.11) cannot be a full description for the DT model, and that nonlinear Eq. (2.10) can, in principle, be a description because the $\nabla^2(\nabla h)^2$ term manifestly breaks the up-down symmetry [46].

Figure 14 shows the height fluctuation distribution functions for DT, 3+, and SOS-MBE growth at 600 K in $2+1$ dimensions [the corresponding MBE growth result in $1+1$ dimension is displayed in the inset of Fig. 14(c)]. The DT and the MBE models show net skewness [13,14] and the distributions are visually asymmetric. In fact, for the saturated DT model ($d = 1+1$) we measure the normalized skewness $\sigma = \langle (h - \bar{h})^3 \rangle / \langle (h - \bar{h})^2 \rangle^{3/2}$ to be negative, reflecting the dominant contribution of the grooves: $\sigma = -0.50 \pm 0.05$. For the discrete LDS model the skewness shows very large fluctuations, and our best estimate for the steady state σ is a small, negative number ($\sigma \approx -0.1 \pm 0.15$) but zero and small positive values are not completely ruled out. The SOS-MBE model at the latest simulation times of Fig. 3 for $T = 600$ and 650 K produces skewed surfaces with $\sigma = -0.49 \pm 0.10$ and -0.44 ± 0.10 , respectively, which is quantitatively consistent with the DT model. Again, this illustrates a quantitative link between the realistic SOS-MBE model and the nonequilibrium DT model, and demonstrates that the purely linear surface-diffusion equation, Eq. (2.11), cannot be the entire story for either model.

As a result of the symmetry breaking, one can see that the asymmetric tail of the distribution becomes im-

portant in calculating the various moments G_q . Such an asymmetric distribution reflects the fact that deep grooves exist in the interface (Fig. 9), and the intermittent step-height fluctuations are manifestations of rare events from the tail of the fluctuation distribution. The 3+ model, which exhibits only the usual self-affine scaling (Fig. 2), has a narrow symmetric step-height distribution

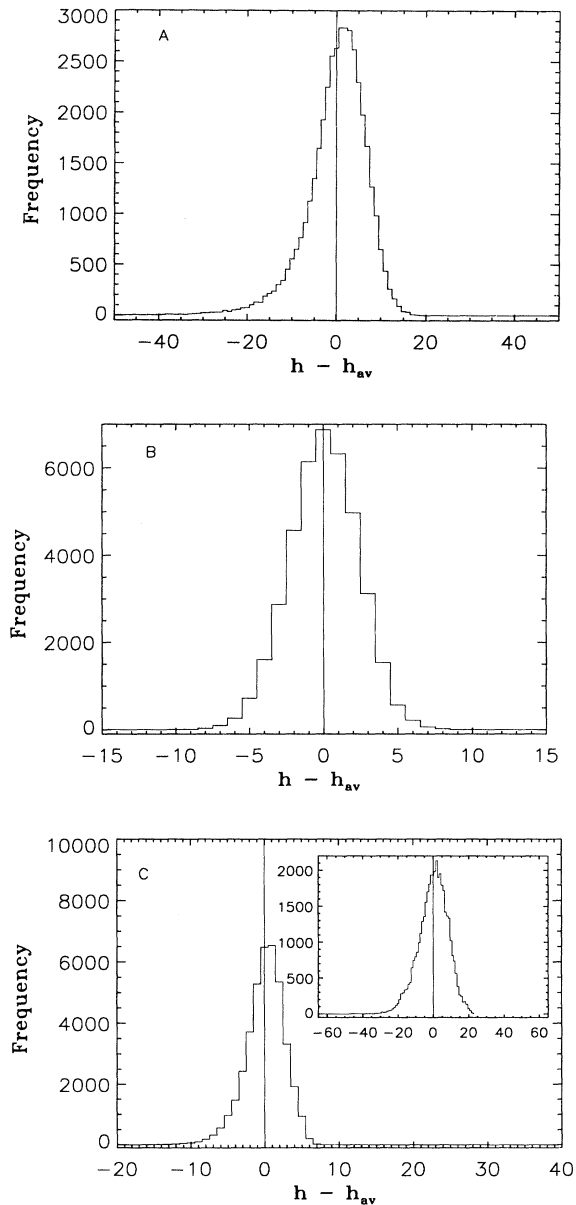


FIG. 14. Height distribution functions around the mean for $L = 200$ in the (a) DT, (b) 3+, and (c) $d = 2 + 1, T = 600$ K SOS-MBE models [the inset of (c) gives $d = 1 + 1, L = 1000, T = 600$ K results]. Only the normally scaling 3+ model has a symmetric distribution function, while a tail for large, negative height fluctuations exists in all other cases.

and no skewness within our error bars. Thus multifractal behavior may have some logical link with the up-down symmetry breaking and asymmetric fluctuations within the subclass of *conservative* growth models (i.e., when BD is excluded).

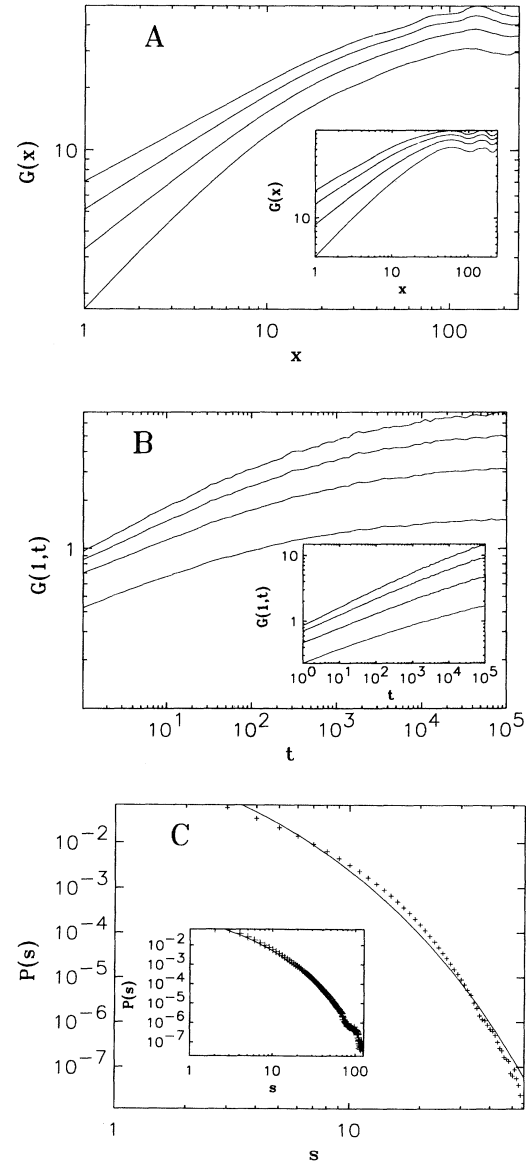


FIG. 15. Comparison of multifractal scaling properties in the LDS and DT (inset) models. (A) Correlation functions $G_q(x, t = 1 \times 10^5)$ vs x for $q = 1, 2, 3, 4$ from bottom to top, where the slope for $x = 1 - 10$ gives α'_q ($L = 500$). (B) The average step height $G_q(1, t)$ vs t , where the slope for $1 \ll t^{1/z} \ll L$ is $\kappa(q)/qz$. These results are ten-run averages, and the q dependence of the exponents extracted appears in Table V. (C) $P(s)$ vs the step size s for $L = 25$, sampling the saturation regime 10^5 times to acquire sufficient statistics. The solid line is a fit to a stretched exponential $C \exp^{-as^\delta}$, where $\delta = 0.47$ (0.42) for LDS (DT).

2. Dynamical models

We have also studied $G_q(x, t)$ for the DT, LDS, TDH, and Family models in $d = 1+1$. Our motivation here is to provide an in-depth analysis of multiaffinity as it arises in models where one has precise control over the microscopic dynamics. We repeat that the signatures of multiaffinity are (i) q -dependent exponents α'_q in the correlation functions $G_q(x, t) \sim x^{\alpha'_q}$ for $x \ll \xi$; (ii) anomalous time dependence of $G_q(1, t) \sim (t^{1/z})^{\kappa(q)/q}$; and (iii) deviation of the step-height distribution function from Gaussian: $P(s) \sim \exp(-as^\delta)$, $\delta < 2$. In Figs. 15(a)–15(c) and in Table V, our simulation data for the LDS model exhibit all three of the above features: (i) α'_q changes from $\alpha'_1 = 0.84$ to $\alpha'_4 = 0.48$; (ii) the value of $\kappa(q)/q$ rises from 0.19 ($q = 1$) to 0.34 ($q = 4$); and (iii) $\delta = 0.47$ provides the best fit to a stretched exponential form for the step distribution function, substantially smaller than the Gaussian value of $\delta = 2$. Since by definition $\alpha = \alpha'_q + \kappa(q)/q$, these results predict that $\alpha = 0.92 \pm 0.10$ for $q = 1-4$, in basic agreement with the prediction of Eq. (2.10), $\alpha = 1$. We extract $\kappa(q)/q$ here from the slope of $G_q(1, t)$ plots, which is in fact $\kappa(q)/zq$; in the LDS (DT) model we take $z = 3$ (4), which are the approximate values we obtain from separate measurements of the global exponents from the t and L dependence of the surface width. Note that these values of z for the LDS and DT model are consistent with the continuum equations (2.10) and (2.11), respectively. For comparison, in the insets of Fig. 15, the same quantities are shown for the DT model using identical growth parameters. Krug [14] has previously examined the DT model for multiaffinity and has found similar quantitative results.

Interestingly, we find in Table V that the functions $G_q(x, t)$ are characterized by essentially identical values of the effective roughness exponent α'_q in DT and LDS models, even though the mean step size $G_q(1, t)$ grows markedly quicker in the DT model and the exponents α and z are very different for the two models. Given the constancy of α'_q in these two models, the change in the

anomalous exponent $\kappa(q)/q$ seemingly reflects the mechanism responsible for changing the growth universality class as manifested through the global roughening exponent α in the DT and LDS models. Table V therefore also gives the quantity $\Delta = [\kappa(q)/q]_{\text{DT}} - [\kappa(q)/q]_{\text{LDS}}$ ($= \alpha_{\text{DT}} - \alpha_{\text{LDS}}$ because of the constancy of α'_q), showing that $\Delta \approx 0.5$, agreeing with the difference in α between the respective universality classes associated with Eqs. (2.11) and (2.10). Note that α is nearly q independent for each model in Table V.

The DT stretching exponent of $\delta = 0.42$ for the step-height distribution function deviates only slightly from the LDS value of 0.47, although the fit to the stretched exponential form is not particularly good for LDS. Nevertheless, the fact that δ decreases is consistent with the increase in $\kappa(q)/zq$ [$G(1, t) \sim t^{\kappa(q)/zq}$] seen in going from the LDS to the DT model, and implies that there are more high steps in the DT model than in the LDS model. The morphologies and step-height profiles in Fig. 9 also demonstrate this behavior. We emphasize that the microscopic difference in the local growth rules between DT and LDS models is in the diffusion of atoms at kink sites, which could potentially be upward in the LDS model: considering Fig. 1(e), only atom a would have a different behavior for the DT model, in which case it would not move. [In the LC model, on the other hand, atom a in Fig. 1(e) would move down, emphasizing that DT, LDS, and LC all obey quite similar but not identical local growth rules.]

In Fig. 16, the behavior of α'_q for a wider range of q in the LDS and DT models is shown and the behavior is similar in the two models, with only minor quantitative differences. In the inset, however, $\kappa(q)/q$ appears very different in the two cases (as it must be in order to produce very different values of α in the two models given an approximately constant α'_q), with the DT model having a well-defined plateau near 0.85 for a wide range of q and dropping sharply for $q < 2$. In the LDS model, the decrease is much smoother due to the lower value of the plateau in $\kappa(q)/q \approx 0.45$. This further emphasizes that these two models are distinguished not by the short-distance spatial scaling of the correlation function,

TABLE V. Multifractal exponents α'_q and $\kappa(q)/q$ for the SOS-MBE ($L = 1000$, $t = 10^5$, $T = 600$ K for $d = 1+1$), LDS, DT, and TDH models in $d = 1+1$ for $q = 1-4$. The data for the dynamical models (all of which have $L = 500$, $t = 10^4$) come from Figs. 15(a,b) and Fig. 19. The quantity $\Delta = [\kappa(q)/q]_{\text{DT}} - [\kappa(q)/q]_{\text{LDS}}$ should be compared with the difference in α between the continuum equations (4) and (3), expected to be 0.5. We note that α'_q is essentially constant for all the models, even the temperature-dependent stochastic models, while $\kappa(q)/q$ is distinguished for the various models. Small quantitative differences between these data and Table III are attributed to finite time effects due to the drastically different system sizes in the two cases.

q	α'_q				$\kappa(q)/q$				α		
	MBE	LDS	DT	TDH	LDS	DT	TDH	Δ	LDS	DT	TDH
1	0.82	0.84	0.85	0.84	0.19	0.59	0.64	0.50	1.03	1.44	1.48
2	0.64	0.67	0.67	0.63	0.25	0.71	0.76	0.46	0.92	1.38	1.39
3		0.56	0.56	0.50	0.30	0.78	0.85	0.48	0.86	1.34	1.35
4	0.50	0.48	0.50	0.43	0.33	0.83	0.90	0.50	0.81	1.33	1.33

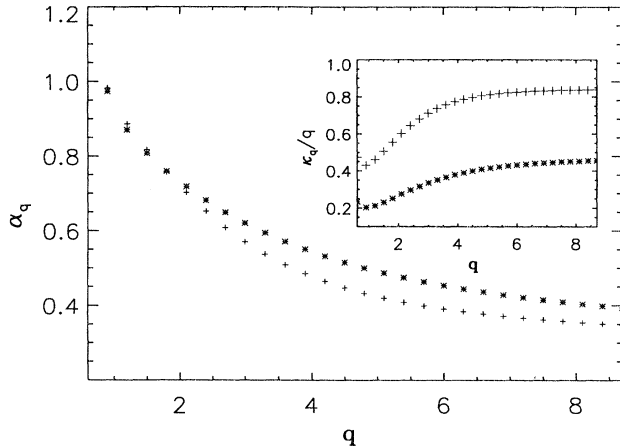


FIG. 16. Expanded q dependence of the exponents α'_q and $\kappa(q)/q$ (inset) for the LDS (*) and DT (+) models. Notice the close correspondence of α'_q for the two models while the plateaus of $\kappa(q)/q$ differ by about 0.5, expected by comparison with continuum equations.

but by the anomalous time scaling in $G(x, t)$ as given in Eqs. (4.1) and (4.3). For the sake of completeness, we show our multiscaling analysis of q th-order correlation functions for the Family model in Fig. 17, and as expected, $\alpha'_q = 0.50 \pm 0.03$ for all q , establishing the existence of only the usual self-affine dynamic scaling in the Family model in sharp contrast to DT and LDS model results of Figs. 15 and 16 (as well as the SOS-MBE results shown earlier) which exhibit multiscaling.

Clear from our results, as has been emphasized in earlier studies [3,5,10–14], is the fact that the DT model does not exactly follow the scaling behavior of linear

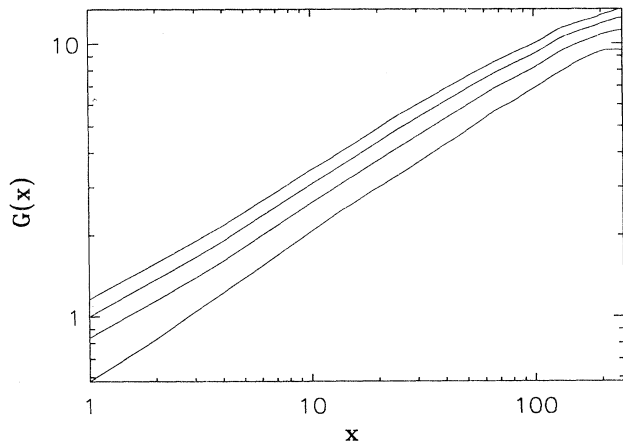


FIG. 17. Correlation function $G_q(x, t = 1 \times 10^6)$ vs x for the Family model with $L = 500$. The near constancy of the slopes for $q = 1, 2, 3, 4$ (from bottom to top) indicates the presence of self-affine scaling, for $\alpha'_1 = 0.53 \pm 0.02$, very close to $\alpha'_4 = 0.48 \pm 0.02$.

Eq. (2.11), as does the LC model. Even though the global exponents α, β , and z of the DT model are surprisingly well described by Eq. (2.11) (at least in an effective sense over many orders of magnitudes of length and time scales), the local exponents α'_q and $\kappa(q)$ are not. Krug found [14] no multifractal behavior in the exponents $\delta, \alpha'_q, \kappa(q)/q$ of the LC model which follows Eq. (2.11) exactly, while the DT model displayed nontrivial q dependence in the higher-order correlation functions. In fact, for linear equations such as Eqs. (2.5) and (2.11), one can show that the growth term renormalizes independently of the noise so that the distribution of step heights $P(s)$ should reflect only the stochasticity of the noise, which in all of our models is δ -function-correlated white noise with a Gaussian distribution. Thus all linear models, or discrete models which obey linear growth equations, must necessarily have $\delta = 2$. This is strong evidence that Eq. (2.11) cannot be the whole story for the DT model, which clearly has an intermittent quality to its step-height distribution function and $\delta < 2$. In addition, the manifest breaking of the $h \rightarrow -h$ symmetry in the DT morphology also indicates that a linear description is not applicable. The very slow crossover associated with $z = 4$, the earlier observation of $\alpha = 1.4 < 1.5$ [3,5], and the decreasing of α for increasingly larger system sizes [5,50] when taken together indicate that the agreement between the linear Eq. (2.11) and the global exponents in the discrete DT model must necessarily be a very long-lived transient. The physical reasons for the crossover time scale in the DT model being exceedingly large ($> 10^8$), and for its global exponents to be so well described by the linear fourth-order Mullins-Herring equation (while at the same time the model exhibiting multifractal behavior, nontrivial anomalous dynamic scaling, and up-down symmetry breaking) are unknown. In fact, we do not know what nonlinear continuum equation the DT model eventually crosses over to because the asymptotic regime has not yet shown up in any simulations.

The question naturally arises as to how the DT model shows global scaling corresponding to Eq. (2.11) (i.e., $\beta \approx 0.375, \alpha \approx 1.4$ [3,5]) and yet generates nontrivial anomalous scaling and multifractal behavior not contained in Eq. (2.11). Theoretically one expects the relevant fourth-order nonlinear term $\lambda_{22} \nabla^2 (\nabla h)^2$ to be the most likely candidate, changing Eq. (2.11) to Eq. (2.10), which has the advantage of breaking the up-down symmetry. But it is puzzling how the nonlinear term could so drastically affect the morphology (Fig. 9), yet be small enough to not show up more clearly in the global scaling exponents. Understanding the q dependence in $\kappa(q)$ and α'_q also remains a serious problem. Indeed, as the deposition shot noise is additive and Gaussian, it is difficult to see it producing the observed non-Gaussian step distributions and the multifractal spectrum, although there has been some very recent theoretical work in this direction [46]. It is possible that the DT model may in a subtle fashion be introducing multiplicative noise, or for reasons not understood yet, cannot be described by a local equation in spite of its growth rules being apparently local. Along these lines, we note that power law noise and quenched noise are both known [39] to gener-

ate nontrivial multifractality in surface growth. One can speculate that there are various random “stable” configurations in the DT morphologies that essentially “pin” the surface at random locations, for example, the bottoms of the large grooves which invariably develop in the DT model (Fig. 9) are candidates for such effective random pinning sites. These sites could perhaps lead to an effective quenched noise because the steep sides prevent diffusion into grooves due to the microscopic rules of the DT model. In this context, we note that DT, WV, and LDS models show anomalous scaling and multifractality, and all develop grooves in their morphologies.

The analogy [14] between height fluctuations in the DT model and the phenomenon of intermittency in fluid turbulence may also help shed some light on the origin of multifractality in these growth models. Intermittency in turbulence refers to the occasional injection of energy from a large-scale structure into a local region, creating structures (e.g., eddies) on the smaller scales. Velocity gradients are created, the magnitudes of which are distributed according to a stretched exponential, and thus very high energy injections (velocity gradients) are rare

but do occur [40,49]. Krug suggested [14] that an analog of intermittency may be responsible for the occurrence of localized regions with very large step heights (Fig. 9) and the stretched exponential form of the step-height distribution function $P(s)$. In the surface growth problem, intermittency may be generated by the noise when a particle happens to land in a site on the interface which has a particular propensity to generate large step heights. Kink sites in the DT model [e.g., particle e in Fig. 1(c)] are candidates for such “intermittent” sites, as they are manifestly stable and can generate higher steps. On the other hand, site b or f in Fig. 1(c), for example, or trapping sites (e.g., the triply bonded site between particles e and f), would not be “intermittency” candidates as they locally do not encourage nonequilibrium structures, but generate smoother morphologies with lower step-height fluctuations. Much more work is clearly needed to clarify the microscopic reasons for the intermittent behavior in the height fluctuations of these models.

We now focus on two modifications of the DT model outlined in Sec. (III A 2). In Fig. 18 and Table VI, we show the behavior of the DT model in the presence of a

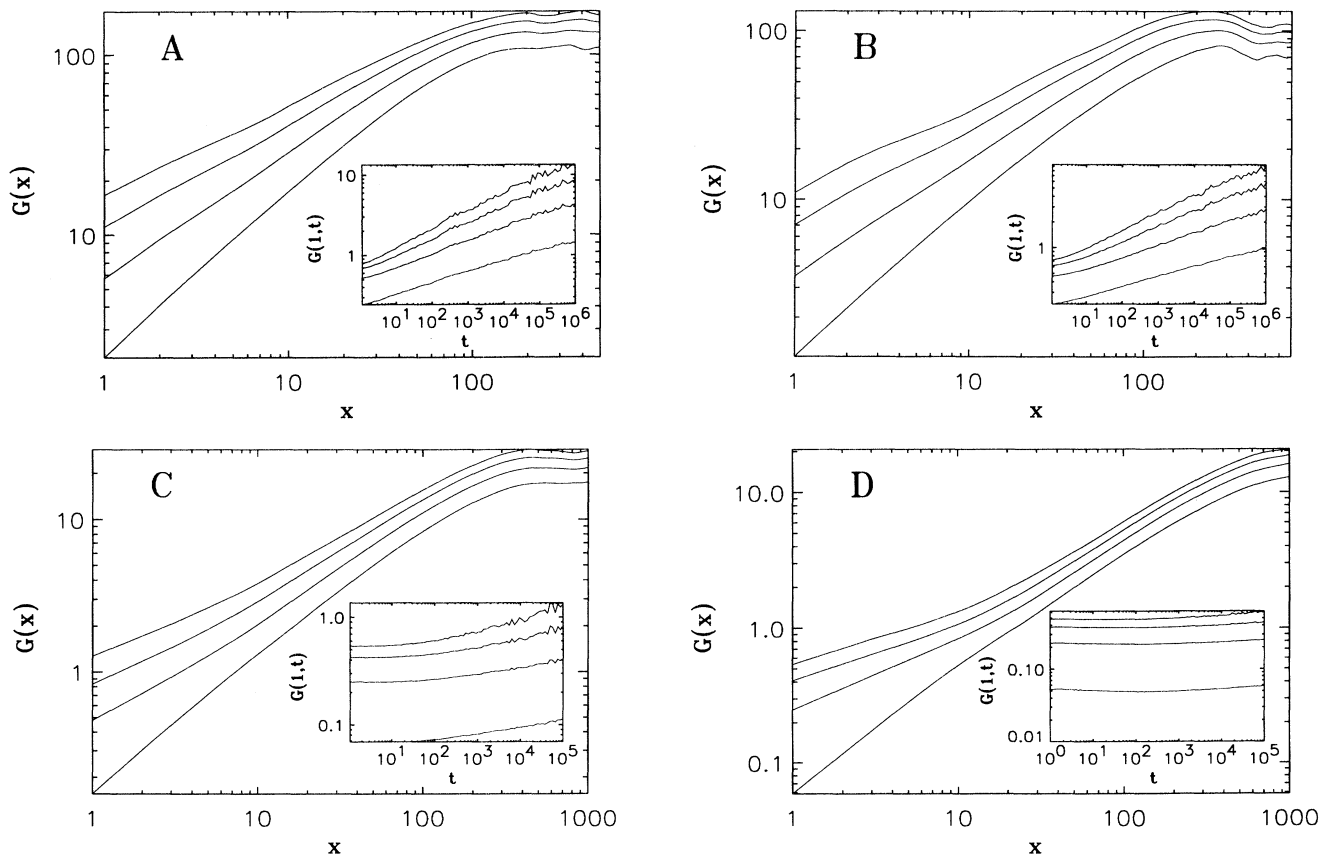


FIG. 18. Multifractional behavior of $G_q(x, t)$ and $G_q(1, t)$ (inset) for the DT model with variable diffusion length. (a) $D = 2$, $L = 1000$, $t_{\max} = 1 \times 10^6$, (b) $D = 3$, $L = 1500$, $t_{\max} = 1 \times 10^6$, (c) $D = 10$, $L = 5000$, $t_{\max} = 1 \times 10^5$, (d) $D = 20$, $L = 10000$, $t_{\max} = 1 \times 10^5$. To measure α'_q , we extract the slope from the $x > D$ region to avoid the finite size effects seen for small x at large D . $\kappa(q)/q$ is measured in the range 10^4 – t_{\max} . The exponents found are tabulated in Table VI. Note that D/L is kept constant.

TABLE VI. Multifractal exponents α'_q and $\kappa(q)/q$ for the $D = 1, 2, 3, 10, 20$ variants of the DT model in $d = 1+1$ for $q = 1-4$. The data for the dynamical models come from Figs. 15(a,b) and Figs. 18(a)–18(d). Here, α'_q is not constant and increases at large D , and the global exponent α falls due to a more rapid decrease of $\kappa(q)/q$.

q	α'_q					$\kappa(q)/q$					α				
	1	2	3	10	20	1	2	3	10	20	1	2	3	10	20
1	0.85	0.89	0.88	0.85	0.83	0.59	0.52	0.53	0.33	0.12	1.44	1.41	1.41	1.18	0.95
2	0.67	0.70	0.68	0.76	0.76	0.71	0.68	0.57	0.36	0.13	1.38	1.38	1.25	1.12	0.89
3	0.56	0.57	0.54	0.68	0.72	0.78	0.80	0.64	0.55	0.14	1.34	1.37	1.18	1.23	0.86
4	0.50	0.50	0.46	0.62	0.67	0.83	0.86	0.71	0.72	0.16	1.33	1.36	1.17	1.34	0.83

variable “diffusion length” $D = 2, 3, 10, 20$ ($D = 1$ corresponds to the original DT model). For values of D up to 3, little qualitative deviation from the DT model in α'_q is detected, although $\kappa(q)/q$ does change noticeably by $D = 3$. For larger D , however, we observe the vanishing of the multiscaling behavior, a qualitative difference signaled by the parallel plots in Fig. 18(d). Here, we find that α'_q actually rises for larger D at a fixed $q > 1$, although the range of α'_q shrinks and, we expect, should collapse to a constant in the $D \rightarrow L$ limit. It is important to note that D represents a new microscopic length scale over which we permit the surface to reorganize, and Figs. 18(a)–18(d) clearly illustrate that this new length scale modifies the behavior of the correlation function. Note that we ignore $x \leq D$ in extracting exponents from these models and keep the L/D ratio fixed by increasing the system size in order to avoid any obvious finite size effects arising from the diffusion length D .

Concurrent with α'_q attaining q independence, $\kappa(q)/q$ falls with increasing D [Table VI and insets of Figs. 18(a)–18(d)] indicating that the average step height may be tending toward saturation. The anomalous scaling of $G_q(1, t)$ weakens in the large D limit, appearing only after ~ 1000 layers for $D = 10, 20$; prior to this time, the large diffusion length permits $G_q(1, t)$ to remain fixed. At $D = 20$, the variation of $\kappa(q)/q$ has sharply contracted to the small range of 0.12–0.16, indicating again that multifractality is giving way to simple self-affinity [$G(1, t) \approx \text{const}$]. We cannot, however, exclude the possibility that the apparent q independence of $\kappa(q)/q$ and the disappearance of multiscaling is a finite time effect, and that for longer simulations one would see $G(1, t)$ rise more sharply. Indeed, $G(1, t)$ appears saturated over almost four orders of magnitude prior to a slight upturn for $D = 20$. Furthermore, another interesting question which remains unanswered in this model is whether anomalous scaling and multifractality are vanishing through independent mechanisms or whether the loss of one necessitates the loss of the other: we believe they are both disappearing due to a single mechanism, for reasons to be elaborated below.

Notice that $\alpha'_q(D = 20) \approx 0.77$ in the DT model is significantly different from the value of $\alpha = \alpha' = 0.50$ in the EW equation. In addition, α'_q is actually *increasing* with D and therefore the DT model with finite diffusion length ($D \leq 20$) is not in the EW universality class. However, we do observe a continuous decrease in the global

roughness exponent α , which falls from ~ 1.4 ($D = 1$) to ~ 0.90 ($D = 20$). While a finite size effect involving the new length scale D will by itself lower the value of α , such a finite size correction should be small here as we have kept the ratio L/D constant at 500 in Fig. 18. We have also attempted to fit the step-height distribution $P(s)$ with the expected stretched exponential form [14] for $D = 10$, to check if the large D limit in some approximation approaches the normal scaling behavior defined by Eq. (3.1). The distribution for $D = 10$ could not be parametrized by a stretched exponential for the full range of parameters [51]. This result and the large value of α'_q can be understood by noting that when D becomes large, the basic DT rule whereby kink sites cannot move still holds so that not all deposited atoms can reach local height minima as they could within the Family model. Thus the WV model [Fig. 1(b)] for $D \rightarrow \infty$ should be a better approximation to the Family model than the DT model in the large D limit. This is consistent with the recent finding that the WV model is asymptotically in the EW universality class [16,35], and another indirect indication that the DT model does not asymptotically possess EW universality.

As opposed to the DT model and the $D > 1$ variant which allows spatially remote regions of the interface to interact at a fixed time, the TDH model examines how “temporally remote” events at a given location on the surface interact by permitting a crude dynamical version of delayed hopping [see Sec. III A 2 and Fig. 1(d) for details]. By allowing atoms to hop at times after their deposition in response to noise-induced changes in the local environment, this model in some sense couples noise and morphology jointly to the dynamics a distance $D + 1$ away. We consider only $D = 1$ in the following discussion for simplicity. The generic multiscaling behavior here is still quite similar to the other DT models studied in this paper (see Fig. 19 and Table V). Quantitatively, α'_q shows a slight decrease from the DT model, while $\kappa(q)/q$ increases by an amount that almost exactly compensates for the drop in α'_q . The best estimates of the exponents are $\alpha \approx 1.6$ and $\beta \approx 0.41$ (approximately consistent with the values in Table III for a larger system), both larger than the corresponding estimates in the DT model [3,5], but they give $z \approx 3.9$, consistent with the DT result. Thus the delayed hopping has increased slightly the global exponents, with little change in the multiscaling exponents. This is somewhat surpris-

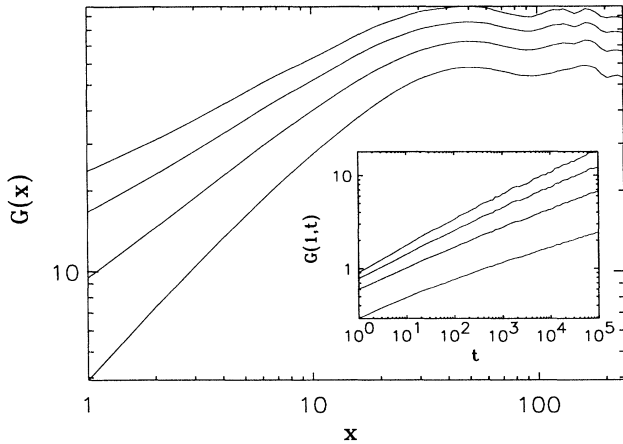


FIG. 19. Multifractal behavior of $G_q(x, t)$ and $G_q(1, t)$ (inset) for the TDH model with $L = 500, t = 10^5$. The resulting exponents are slightly larger than in the DT model; see Table VI.

ing as one would have expected the interface to become smoother as a result of the additional relaxational mode in the TDH model.

The SOS-MBE, DT, DT with $D > 1$, LDS, and TDH models all possess both multifractality and anomalous scaling behavior, but as noted above, these two features are, in principle, independent characteristics: depending upon the details of the growth model both, one, or none of these characteristics may show up (with the caveat that we believe anomalous scaling to be a necessary prerequisite for multifractality). For example, the DT model has both, the Family model has neither, and the LC model [13] exhibits anomalous scaling but not multiscaling. Recall that the LC model exactly follows the fourth-order *linear* continuum equation [13,14], Eq. (2.11), with $\kappa = 1$ and $\alpha' = 1$ for all q , and has up-down symmetric morphologies [52]. The Family model, which follows exactly the linear EW equation, our Eq. (2.5), shows neither anomalous scaling nor multiscaling. Nonlinear terms in *conservative* continuum equations are responsible for generation of $h \rightarrow -h$ symmetry breaking and, we suspect, multifractality. But, again, the breaking of up-down symmetry does not necessarily imply anomalous scaling or multifractality—the KPZ equation does not show anomalous scaling or multifractality in any physical dimensions (certainly not in $d = 1 + 1$), but the second-order nonlinearity, Eq. (2.1), obviously breaks the up-down symmetry. We are not aware of any model possessing multiscaling, but lacking anomalous scaling and broken up-down symmetry. We therefore believe that anomalous scaling and broken up-down symmetry (i.e., skewness in the growing interface) are absolutely necessary conditions for the existence of multifractality in growth models; either alone does not seem sufficient (cf. the LC and BD models). Evidently, rather nontrivial nonlinear growth terms are necessary to produce multifractality [while anomalous scaling, i.e., $\alpha' < \alpha$ and $\kappa > 0$, is triv-

ially present in any growth model with $\alpha > 1$, e.g., Eq. (2.11)], but the sufficient conditions needed to produce multiscaling in surface growth models are not yet known [46].

We conclude this section by emphasizing that our numerical results support the original contention [3,5] that the instantaneous-relaxation DT-type dynamical models (and its variants such as LDS, DT with finite diffusion lengths, TDH, etc.), which emphasize local coordination or bonding-driven atomic diffusion, catch the essential qualitative and quantitative aspects of the minimal SOS-MBE kinetically rough growth model with temperature-activated Arrhenius hopping of all atoms at the growth front. In particular, the global exponents α and β of the full SOS-MBE growth model (Table III) are reasonably close to those of the DT model (Table IV) with $D = 1$ or the DT model with $D > 1$ (Table VI) depending on the growth temperature (at higher growth temperatures diffusion length is enhanced, making the DT model with $D > 1$ the more appropriate model). The correlation roughness exponent $\alpha' \equiv \alpha'_{q=2}$, which is experimentally relevant, is essentially the same (within error bars) in the DT model ($\alpha' = 0.67$) as in the SOS-MBE growth model ($\alpha' = 0.64 - 0.61$) over the time scale considered. This agreement in the anomalous scaling behavior of the DT model with the full SOS-MBE model reinforces the contention that critical properties of MBE growth (at least in the kinetically rough low temperature regime) are well described by the nonequilibrium DT model. What we find truly remarkable is that the multiscaling exponent α'_q (Table V) is essentially the same numerical value for each q in Table V for all five SOS growth models we study here: full MBE, DT, LDS, TDH, and DT with $D < 10$ (Table VI). Because α'_q is an important exponent characterizing anomalous scaling and multifractality in our growth models as well as being experimentally the most accessible, its numerical uniformity in all our MBE growth models (*including* the stochastic temperature-dependent model) strongly suggests that there may very well be a single underlying long-wavelength description for all of these diffusion-driven models (including the SOS-MBE model), and the differences in the observed global exponents among these models (with SOS-MBE being in the “DT universality” in $d = 1 + 1$ and in the “LDS universality” in $d = 2 + 1$ according to Table III) could be arising from slow crossover and finite size effects. The fact that SOS-MBE may have different “universalities” in different dimensions and that the surface-diffusion-driven growth models (DT, LDS, WV, SOS-MBE, etc.) may have slow crossover effects have earlier been noted in the context of other simulation studies [4,5,10,22,35]. Our work here establishes that the similarities between temperature-dependent stochastic Arrhenius SOS-MBE growth simulations and those based on instantaneous-relaxation DT-type dynamical growth models encompass both global and local scaling exponents as well as morphologies, anomalous and multiscaling behaviors. Thus in order to understand minimal MBE growth we must first develop a complete understanding of the simpler DT dynamical model.

As emphasized throughout this paper and elsewhere

[10–14] we do not yet have a full understanding of the DT model. In fact, we do not even know whether a coarse-grained continuum description exists for this deceptively simple model. It is hard to see how simple local growth rules, which in the case of the DT model are inspired by the physics of MBE, could be lacking a long-wavelength continuum description. One difficulty is that the DT rules [Fig. 1(c)] do not have any simple local geometrical interpretation in terms of local height or local curvature as the Family [Fig. 1(a)] or LC models [Fig. 1(f)] do. In particular, Kim and Das Sarma showed [13] quite generally the connection between local geometric rules involving height, curvature, etc. and the continuum growth equation, and it is clear that while DT-type models obey many features of the curvature-driven model there are significant differences. The current belief [14,46] is that if a continuum description for the DT model exists, then it probably involves an infinite series of relevant terms. For example, the following equation has recently been suggested [46] as a possible long-wavelength continuum description of DT-type models (and therefore by inference of SOS-MBE growth):

$$\partial h/\partial t = -\lambda_4 \nabla^4 h + \sum_{n=1}^{\infty} \lambda_{2n} \nabla^2 (\nabla h)^{2n} + \eta_F, \quad (4.4)$$

where if we keep only the first term in the infinite series we get our Eq. (2.10), which has been much discussed in the recent literature [8,9,29,30]. We note the obvious fact that the growth coefficients λ_{2n} are manifestly nonequilibrium and must therefore vanish in the limit of zero flux ($F \rightarrow 0$). Further discussion of this topic [14,46] is well beyond the scope of this article.

V. CONCLUSION

We first summarize the principal findings reported in this paper. (1) The critical exponents and morphologies of minimal SOS-MBE growth are well described by the nonequilibrium DT growth model at least in the intermediate temperature range where finite size effects are minimized. The MBE growth universality at low to intermediate temperatures is therefore most likely the same as the DT universality. (2) The equivalence between these two models extends from the approximate numerical agreement in the global exponents (α, β) characterizing the dynamics of interface width fluctuation all the way to the anomalous scaling and multiscaling exponents $\alpha'_q = \alpha - \kappa(q)/q$ characterizing the higher moments of height difference correlation functions. (3) We show that the SOS-MBE model as well as a whole class of surface-diffusion-driven discrete dynamical growth models (Fig. 1), namely, LDS, DT with finite diffusion length, and TDH models have anomalous and multiaffine scaling properties very similar to those in the DT model [14], and they all exhibit the intermittent height fluctuation behavior with a stretched exponential step-size distribution function. In addition, we find that all these models have exactly the same multiscaling exponent α'_q for various q 's, implying the possible existence of one underlying

theoretical universality class for all of these models (including SOS-MBE). Our numerical results are inconsistent with the asymptotic universality class being described by any of the continuum equations discussed in Sec. II of this paper, although the fourth-order continuum equations [i.e., Eqs. (2.10) and (2.11)] provide good agreement with our calculated global growth exponents. None of the SOS models studied in this paper (except for the Family model) seems to belong to the EW universality of Eq. (2.5). (4) Our BD-MBE stochastic simulation results show the expected KPZ behavior asymptotically; however, the preasymptotic crossover is slow and dominated by the SOS behavior found in our SOS-MBE simulations, and can thus mimic SOS-MBE in early time regimes.

There has been extensive recent experimental activity measuring MBE growth exponents [53–71] following the suggestions of Refs. [3,7–9] that MBE growth may not belong to the generic second-order continuum growth model. Most of these experiments conclude that MBE growth exponents are well described by fourth-order continuum growth equations such as Eqs. (2.10) and (2.11), with $\beta \approx 0.2$ – 0.25 and $\alpha(\alpha')$ large (close to unity) in $d = 2 + 1$. Qualitatively, therefore, these experimental findings are completely consistent with the results presented in this paper—in particular, our conclusion that the DT model is the appropriate MBE growth model is approximately consistent with experimental findings. (We should emphasize that all the experimental results, except for one [61] which actually is a BD-MBE growth experiment, are for $d = 2 + 1$ growth and most of our numerical results [37] are for $d = 1 + 1$.) On closer inspection, however, we find the experimental situation quite unconvincing because none of the experimental results definitively establishes the existence of scale invariance in MBE growth in a large enough range of parameters to satisfy us that the measured exponents are meaningful (rather than wishful). The only compelling conclusion from these experimental studies that we draw is that kinetically rough SOS-MBE growth is substantially rougher (in the thermodynamic limit) than that implied by the generic second-order EW and KPZ models, and the proposed surface-diffusion-driven growth models (e.g., DT, LDS, etc.) with the associated fourth-order continuum equations, Eqs. (2.10) and (2.11), may have some relevance to real MBE growth.

The implications of anomalous scaling for experimental observations of various exponents are potentially important. In many experiments, the roughness exponent is measured from the width W as a function of a window size (*not* the system size L), or from the height-height correlation function $G(x, t)$. In these cases, it is the anomalous roughness exponent α' for the correlator which is being measured [see Eq. (4.1)]. Alternatively, the structure factor $S(k) \sim k^{-\gamma}$ could be employed to give the exponent α' from the relation $2\alpha' + d' = \gamma$. The measurement of the growth exponent β is most often accomplished by analyzing the time dependence of the evolving width. The exponents typically quoted for continuum equations, though, are α and β , *not* α' and β . [In fact, for nonlinear equations, such as Eq. (2.10), α' is not *exactly* known

theoretically even though it is expected to have only logarithmic corrections to unity [46].] With the measured combination of α' and β , one does not know the true dynamic exponent $z = \alpha/\beta \neq \alpha'/\beta$ if $\alpha \neq \alpha'$ (i.e., if there is anomalous scaling). In the presence of anomalous scaling the parameter $z_1 = \alpha'/\beta$ is always an underestimate of the exponent z relevant to the various continuum equations (see Table III). For our SOS-MBE models, $z_1 \approx 1.7$, which is even less than $z_{EW} = 2$. If this value of z_1 is compared with the theoretical models, *assuming that* $z_1 = z$, one would erroneously conclude that the simple Edwards-Wilkinson universality is present. One therefore needs to know whether anomalous scaling occurs in the experimental situation to interpret the data. When anomalous scaling occurs, either α must be measured directly [from $W(L, t)$ data, for example] or κ must be found to convert α' to α . Investigating $G(1, t) \sim t^{\kappa/z}$ tells us if anomalous scaling is present. In particular, scaling is anomalous if one finds κ to be non-zero. Because the solid-on-solid minimal MBE model with activated diffusion has long been the paradigm for modeling detailed material specific situations, we feel that our scaling findings for the MBE model may in fact reflect aspects of the true underlying dynamical behavior (i.e., that in real systems $\kappa \neq 0$ so that $\alpha' \neq \alpha$). Thus it is important for experimental studies to extract a single set of exponents (α, β, z , for example) where we reiterate that the distinction between the primed and unprimed exponents is that the unprimed exponents assume time is measured in layers, while the primed exponents assume time is the reduced time t_r defined following Eq. (4.3). Few experimental studies consider these subtleties in interpretations of the data.

Another possible complication in interpreting experiment is the interplay between the deposition and the diffusion noise. Asymptotically the nonconserved deposition noise η_F always determines the growth exponents, but for short length scales $x < l$ (where l is the diffusion length [28]) the conserved diffusion noise η_D dominates the crossover behavior. The growth exponents corresponding to Eqs. (2.10) and (2.11) with only conserved noise (i.e., $\eta_F = 0$ and $\eta \equiv \eta_D$) are known [33]:

$$\begin{aligned} \alpha &= (2 - d')/3, \quad \beta = (2 - d')/(10 + d'), \\ z &= (10 + d')/3 \end{aligned} \quad (5.1)$$

corresponding to Eq. (2.10), and

$$\alpha = (2 - d')/2, \quad \beta = (2 - d')/8, \quad z = 4 \quad (5.2)$$

corresponding to Eq. (2.11). [For the sake of completeness, we mention that EW growth, Eq. (2.5), driven only by conserved noise, is completely smooth with no kinetic roughness whatsoever for both $d' = 1, 2$.] The diffusion length l increases [28] exponentially with increasing temperature and therefore at higher temperatures (and low deposition rates) one may be dominated by conserved noise crossover behavior defined by Eq. (5.2) or Eq. (5.2). We further note that the growth exponents for conserved diffusion noise are substantially smaller than those for the nonconserved deposition noise [e.g.,

$\alpha = 1/3$ (0), $\beta = 1/11$ (0) in $d' = 1$ (2) for conserved noise in Eq. (2.10) as against $\alpha = 1$ (2/3), $\beta = 1/3$ (1/5) for unconserved noise], which may be part of the reason why finite temperature SOS-MBE simulations consistently produce (cf. Table III) growth exponents somewhat lower in numerical value than the corresponding DT-LDS model results. (We emphasize that by construction instantaneous-relaxation dynamical models have no diffusion noise.) Invariably the presence of some conserved diffusion noise leads, therefore, to somewhat lower crossover growth exponents than the true asymptotic exponents, further complicating interpretation of realistic simulational (or, experimental) results in molecular beam epitaxy. Note that, in general, the diffusion length l is a very complicated and unknown function of growth temperature and deposition rates [28]. Of course, at very high (low) growth temperatures and/or very low (high) deposition rates, there are rather trivial crossover effects in MBE growth arising from local equilibration (purely random deposition) which are easy to discern.

In conclusion, we have demonstrated (conclusively in $d = 1 + 1$, somewhat tentatively in $d = 2 + 1$) that for finite temperature minimal MBE growth models with activated diffusion in the SOS approximation and for several relevant surface-diffusion-driven dynamical models, the usual dynamic scaling ansatz does not apply. The modified ansatz of anomalous scaling works well over a long range of time (whether this is a very long-lived transient or not is unknown at the present time). In this time range, the exponents α' and z' defined by the dynamical scaling form of Eq. (4.1)–(4.3) turn out to be temperature independent in our SOS simulations for $d = 1 + 1$ and $2 + 1$, and surprisingly close to α'_2 in all the relevant dynamical models. In fact, extensive study of anomalously scaling dynamical models indicates that they are distinguished not by the x dependence of the correlation function, but by the anomalous time dependence of the average step height through the anomalous exponent κ . In the finite temperature ballistic deposition model, no anomalous scaling appears asymptotically, although before crossing over to the eventual KPZ universality, the scaling function exhibits many characteristic features of the stochastic SOS-MBE model.

The SOS-MBE models also show multiaffinity, which is associated with the asymmetric distribution of the height fluctuations when manifestly nonequilibrium nonlinearities are present in a *conservative* continuum growth description. All the surface-diffusion-driven discrete dynamical models we study also show multiaffinity under these same general conditions; only LC and Family models, which obey *linear* continuum equations, do not. Dynamical models with multiaffinity necessarily display an up-down asymmetry in the observed morphologies and anomalous scaling, leading to the speculation that the existence of such features is a necessary condition for multiaffinity. The presence of nonequilibrium nonlinearities in the corresponding continuum description may also be a sufficient condition for multiaffinity. Based on these ideas, we believe that the DT model, sometimes considered to follow the linear Eq. (2.11), must cross over asymptotically to some other nonlinear nonequilibrium

continuum description [perhaps to Eq. (4.4)], in keeping with the observed multiaffinity and nontrivial anomalous scaling. When the diffusion length D in the DT model is increased, an interesting increase of the global exponents has been observed, and in the range of D studied, the multiaffine exponents α'_q in the models moved away from those of the EW universality class, a further indication that it is unlikely that the DT model, even in the large D limit, belongs to the EW universality. The TDH model with delayed hopping also shows anomalous roughening and multiscaling, but generates a slightly rougher interface than the pure DT model. Considering all these factors which can lead to nontraditional scaling, it is clear that experimentally measured exponents could easily lead to wrong conclusions regarding the dynamical universality class of kinetic roughening unless care is taken to study subtle aspects of anomalous scaling in interpreting data.

Our most important qualitative conclusion is that the simple DT model describes very well the critical aspects of the minimal SOS-MBE growth scenario, with the two (DT, SOS-MBE) models showing identical (in a statistical sense) features for both anomalous scaling properties and multiaffinity. Our understanding of scale invariance and dynamical correlations in models of molecular beam epitaxy is far from complete, however, because we do not yet have a firm quantitative explanation for the details of even the deceptively simple DT model. In particular, the continuum growth equation underlying the DT model is not yet decisively known, even though it is clear the generic second-order EW equation, Eq. (2.5), does not work, and that the fourth-order continuum equations [Eqs. (2.10) and (2.11)] must be playing an important role. Much more work will be needed before we develop a complete understanding of MBE growth models—in par-

ticular, the nature of anomalous scaling and multiscaling in these models remains intriguing even though the details provided in this paper give a rather complete description (for flat substrates in the absence of Schwoebel barriers) of the phenomenology in $d = 1 + 1$ dimensions. Correspondingly detailed calculations in $d = 2 + 1$ are not currently feasible and considerable work will be needed to completely elucidate the possible anomalous and multiscaling behavior in three-dimensional MBE growth. Unfortunately, that work awaits a many-fold increase in the speed of computation, because the results presented in this article already push the limits of currently available state of the art workstations, parallel processing machines, and supercomputers. Based on extensive numerical results presented in this article our best current guess for the MBE continuum growth equation is Eq. (4.4) at low (high) temperatures (growth rates), with perhaps $\nu_2 \nabla^2 h$ and $\lambda_{13} \nabla(\nabla h)^3$ growth terms of Eq. (2.3) showing up (with very small numerical values of the coefficients ν_2 and λ_{13}) at higher (lower) temperatures (growth rates) as multiple bond breaking processes get activated. Very recent theoretical work [46] indicating the possible existence of anomalous scaling [72] and multiaffinity in Eq. (4.4) provides some support [73] for this speculation, but more work is needed before a definitive statement can be made about the MBE growth equation.

ACKNOWLEDGMENTS

We thank Dr. P. I. Tamborenea and Professor J. M. Kim for many helpful comments and conversations over the course of this work. This work is supported by the United States Office of Naval Research (US-ONR).

-
- [1] A. Madhukar and S.V. Ghaisas, *CRC Crit. Rev. Solid State Mater. Sci.* **13**, 1434 (1987); A. Rockett, *J. Vac. Sci. Technol. B* **6**, 763 (1988); T. Kawamura, A. Kobayashi, and S. Das Sarma, *Phys. Rev. B* **39**, 12723 (1989); D.D. Vvedensky and S. Clarke, *Surf. Sci.* **225**, 373 (1990); I.K. Marmorosk and S. Das Sarma, *Phys. Rev. B* **45**, 11 262 (1992); references therein.
 - [2] S. Das Sarma, *J. Vac. Sci. Technol. A* **8**, 2714 (1990); S. Das Sarma, *J. Vac. Sci. Technol. B* **10**, 1695 (1992).
 - [3] S. Das Sarma and P.I. Tamborenea, *Phys. Rev. Lett.* **66**, 325 (1991).
 - [4] D. Wilby, D.D. Vvedensky, and A. Zangwill, *Phys. Rev. B* **46**, 12 896 (1992).
 - [5] P.I. Tamborenea and S. Das Sarma, *Phys. Rev. E* **48**, 2575 (1993).
 - [6] L. Golubovic and R. Bruinsma, *Phys. Rev. Lett.* **66**, 321 (1991).
 - [7] D. Wolf and J. Villain, *Europhys. Lett.* **13**, 389 (1990).
 - [8] Z.W. Lai and S. Das Sarma, *Phys. Rev. Lett.* **66**, 2348 (1991).
 - [9] J. Villain, *J. Phys. (France) I* **1**, 19 (1991).
 - [10] S. Das Sarma and S.V. Ghaisas, *Phys. Rev. Lett.* **69**, 3762 (1992); **71**, 2510 (1993); M. Plischke, J.D. Shore, M. Schroeder, M. Siegert, and D.E. Wolf, *ibid.* **71**, 2509 (1993); M. Kotrla, A.C. Levi, and P. Smilauer, *Europhys. Lett.* **29**, 25 (1992).
 - [11] S. Das Sarma, S.V. Ghaisas, and J.M. Kim, *Phys. Rev. E* **49**, 122 (1994).
 - [12] M. Schroeder, M. Siegert, D.E. Wolf, J.D. Shore, and M. Plischke, *Europhys. Lett.* **24**, 563 (1993); to mitigate any confusion, we note that the convention in defining the primed and unprimed variables in this reference is *opposite* to that used here.
 - [13] J.M. Kim and S. Das Sarma, *Phys. Rev. Lett.* **72**, 2903 (1994).
 - [14] J. Krug, *Phys. Rev. Lett.* **72**, 2907 (1994).
 - [15] J.G. Amar, P.M. Lam, and F. Family, *Phys. Rev. E* **47**, 3242 (1993).
 - [16] J. Krug, M. Plischke, and M. Siegert, *Phys. Rev. Lett.* **70**, 3271 (1993).
 - [17] F. Family, *J. Phys. A* **19**, L441 (1986).
 - [18] S.F. Edwards and D.R. Wilkinson, *Proc. R. Soc. London, Ser. A* **381**, 17 (1982).
 - [19] D. Kessler, H. Levine, and L.M. Sander, *Phys. Rev. Lett.*

- 69**, 100 (1992); H. Yan, *ibid.* **68**, 3048 (1992).
- [20] M. Kardar, G. Parisi, and Y.C. Zhang, *Phys. Rev. Lett.* **56**, 889 (1986).
- [21] D.D. Vvedensky, A. Zangwill, C.N. Luse, and M.R. Wilby, *Phys. Rev. E* **48**, 852 (1993).
- [22] S. Das Sarma, C.J. Lanczycki, S.V. Ghaisas, and J.M. Kim, *Phys. Rev. B* **49**, 10693 (1994).
- [23] M. Siegert and M. Plischke, *Phys. Rev. Lett.* **73**, 1517 (1994); A.W. Hunt, C. Orme, D.R.M. Williams, B.G. Orr, and L.M. Sander, *Europhys. Lett.* **27**, 611 (1994).
- [24] C.J. Lanczycki and S. Das Sarma (unpublished).
- [25] C.J. Lanczycki and S. Das Sarma, *Phys. Rev. E* **50**, 213 (1994).
- [26] M. Kardar and J.O. Indekeu, *Europhys. Lett.* **12**, 161 (1990).
- [27] S. Das Sarma, *Fractals* **1**, 784 (1993).
- [28] S.V. Ghaisas and S. Das Sarma, *Phys. Rev. B* **46**, 7308 (1992).
- [29] J.M. Kim and S. Das Sarma, *Phys. Rev. E* **51**, 1889 (1995).
- [30] S. Das Sarma and R. Kotlyar, *Phys. Rev. E* **50**, R4275 (1994).
- [31] J.A. Stroschio, D.T. Pierce, M. Stiles, A. Zangwill, and L.M. Sander (unpublished).
- [32] C. Herring, *J. Appl. Phys.* **21**, 301 (1950); W.W. Mullins, *ibid.* **28**, 333 (1957).
- [33] The $\nabla^2(\nabla h)^2$ nonlinearity of Eqs. (2.3) and (2.10) was first introduced into growth equations by T. Sun, H. Guo, and M. Grant [*Phys. Rev. A* **40**, 6763 (1989)] as a conserved KPZ nonlinearity with the noise η considered a completely conserved noise $\eta \equiv \eta_D$. In contrast, the deposition noise is unconserved in the MBE growth situation as emphasized in Refs. [8,9].
- [34] J. Krim and J.O. Indekeu, *Phys. Rev. E* **48**, 1576 (1993).
- [35] P. Šmilauer and M. Kotrla, *Phys. Rev. B* **49**, 5769 (1994).
- [36] S. Das Sarma and P.I. Tamborenea, *Phys. Rev. B* **46**, 1925 (1992).
- [37] C.J. Lanczycki and S. Das Sarma, *Phys. Rev. B* **51**, 4579 (1995).
- [38] M. Schimschak and J. Krug (unpublished).
- [39] A. Barabási, P. Szépfalussy, and T. Vicsek, *Physica A* **178**, 17 (1991).
- [40] P. Kailasnath, K.R. Sreenivasan, and G. Stolovitzky, *Phys. Rev. Lett.* **68**, 2766 (1992).
- [41] J.M. Kim and S. Das Sarma (unpublished); J. Krug (unpublished).
- [42] J. Krug and H. Spohn, in *Solids Far From Equilibrium*, edited by C. Godrèche (Cambridge University Press, Cambridge, England, 1992); references therein.
- [43] C.J. Lanczycki and S. Das Sarma (unpublished).
- [44] H. Leschhorn and L.-H. Tang, *Phys. Rev. Lett.* **70**, 2973 (1993).
- [45] The same is true for all the higher-order *linear* models of the ∇^{2n} type with $n \geq 2$, all of which have $\alpha' = 1$ and $\alpha = (n - 1/2)$, making $\kappa = (2n - d - 1)$ for $n \geq 2$ and $d = 1 + 1$ or $2 + 1$. Note that in $d = 2 + 1$ the ∇^4 linear model has a logarithmic anomalous scaling exponent with $\kappa = 0^+$.
- [46] J.K. Bhattacharjee, S. Das Sarma, and R. Kotlyar (unpublished).
- [47] While the scaling collapse of Fig. 6 for the BD model does not have the high quality of the corresponding SOS scaling collapses in Figs. 3 and 4, saturation of the scaling function is clear in Fig. 6 and the deviations for $y = 0.1 \rightarrow 1.0$ are attributed to the intrinsic width and defect formation effects, well known to be important for non-conservative growth, and demonstrate a problem of using a single-valued height function to describe BD growth. See Refs. [22,37,42], for example.
- [48] We note that the correlation lengths in the simulations yielding α' and z' are small [$\xi(t_{\max}) \sim 30\text{--}60$ for the data of Fig. 5(a)] compared to the largest system size ($L = 200$) used to extract an L -independent value for γ in Fig. 7(a), so the comparison between γ and z' may not be completely justified due to finite size effects. In particular, we note that for $L = 50$ in the $d = 1 + 1$ results for $S(k)$ [so that $L \approx \xi(t_{\max})$], $\gamma \approx 2.3$, the finite size effect making γ more consistent with z' . Because growth in $2 + 1$ dimensions is not as constrained as it is for $d = 1 + 1$ (there are more diffusional opportunities for an atom in higher dimensions), it seems reasonable that such effects are reduced.
- [49] D. Lohse and S. Grossmann, *Physica A* **194**, 519 (1993).
- [50] P.I. Tamborenea and S. Das Sarma (unpublished).
- [51] We attempted to fit the $P(s)$ distribution to the stretched exponential form, but very few step-height values occur even for very long simulations both in the $D = 10, 20$ DT model and the Family model, and such an exercise is not statistically meaningful.
- [52] J.M. Kim (private communication).
- [53] E.A. Eklund, R. Bruinsma, J. Rudnick, and R.S. Williams, *Phys. Rev. Lett.* **67**, 1759 (1991).
- [54] R. Chiarello, V. Panella, J. Krim, and C. Thompson, *Phys. Rev. Lett.* **67**, 3408 (1991).
- [55] J. Chevrier, V. Le Thanh, R. Buys, and J. Derrien, *Europhys. Lett.* **16**, 737 (1991).
- [56] E.A. Eklund, E.J. Snyder, and R.S. Williams, *Surf. Sci.* **285**, 157 (1993).
- [57] R.C. Salvarezza, L. Vázquez, P. Herrasti, P. Ocón, J.M. Vara, and A.J. Arvia, *Europhys. Lett.* **20**, 727 (1992).
- [58] J. Krim, I. Heyvaert, C. Van Haesendonck, and Y. Bruynseraede, *Phys. Rev. Lett.* **70**, 57 (1993).
- [59] Y.-L. He, H.-N. Yang, T.-M. Lu, and G.-C. Wang, *Phys. Rev. Lett.* **69**, 3770 (1992).
- [60] M.A. Cotta, R.A. Hamm, T.W. Staley, S.N.G. Chu, L.R. Harriott, and M.B. Panish, *Phys. Rev. Lett.* **70**, 4106 (1993).
- [61] F. Wu, S.G. Jaloviar, D.E. Savage, and M.G. Lagally, *Phys. Rev. Lett.* **71**, 4190 (1993).
- [62] V. Panella and J. Krim, *Phys. Rev. E* **49**, 4179 (1994).
- [63] H.-J. Ernst, F. Fabre, R. Folkerts, and J. Lapujoulade, *Phys. Rev. Lett.* **72**, 112 (1994).
- [64] M.D. Johnson, C. Orme, A.W. Hunt, D. Graff, J. Sudijono, L.M. Sander, and B.G. Orr, *Phys. Rev. Lett.* **72**, 116 (1994).
- [65] H.-J. Ernst, F. Fabre, R. Folkerts, and J. Lapujoulade, *J. Vac. Sci. Technol. A* **12**, 1809 (1994).
- [66] W.M. Tong, R.S. Williams, A. Yanase, Y. Segawa, and M.S. Anderson, *Phys. Rev. Lett.* **72**, 3374 (1994).
- [67] K. Fang, T.-M. Lu, and G.-C. Wang, *Phys. Rev. B* **49**, 8331 (1994).
- [68] G.W. Collins, S.A. Letts, E.M. Fearon, R.L. McEachern, and T.P. Bernat, *Phys. Rev. Lett.* **73**, 708 (1994).
- [69] P.P. Swaddling, D.F. McMorrow, R.A. Cowley, R.C.C. Ward, and M.R. Wells, *Phys. Rev. Lett.* **73**, 2232 (1994).
- [70] G. Palasantzas and J. Krim, *Phys. Rev. Lett.* **73**, 3564

(1994).

- [71] H. Zeng and G. Vidali, *Phys. Rev. Lett.* **74**, 582 (1995).
- [72] We mention that the anomalous scaling ansatz as defined by Eqs. (4.1)–(4.3) has some formal similarities with critical phenomena in the presence of a *dangerous irrelevant field*. In particular, the scaling form of Eq. (4.2), $G(x, t) = x^{2\alpha} \hat{g}(x/t^{1/z})$, with $\hat{g}(y \ll 1) = y^{-\kappa}$ in the anomalous scaling situation instead of $\hat{g}(y \ll 1) = 1$ in the normal, self-affine scaling situation, is similar to the critical behavior associated with a dangerous irrelevant variable. The important aspect of our problem is that the nonzero value of the anomalous exponent κ not only indicates an “anomalous” scaling function for $y = x/t^{1/z} \rightarrow 0$ (exactly the same way as in the dangerous irrelevant variable case) but also signifies a physical difference in the local and the global dynamic scaling behavior of the growth interface as the dynamical interface width and the height-height correlation function scale with *different* roughness exponents α and $\alpha' = \alpha - \kappa/2$, respectively. In contrast, dangerous irrelevant variables only modify the asymptotic scaling function and do not affect any critical exponents. (We thank M.E. Fisher for a discussion on this point.)
- [73] It is easy to show that *within the perturbative DRG theory* all the nonlinear $\lambda_{2n} \nabla^2 (\nabla h)^{2n}$ terms in Eq. (4.4)

are relevant and have exactly the same global critical exponents in $d' = 1$ as the leading-order Lai–Das Sarma–Villain nonlinearity $\lambda_2 \nabla^2 (\nabla h)^2$ considered in Ref. [8]. In $d' = 2$ the higher-order nonlinearities ($n > 1$) are marginal, and the perturbative DRG exponents are given by the leading-order nonlinearity. One finds the following exact results for $d' \geq 1$ for Eq. (4.4) within the perturbative DRG theory: $z = [4(n+1) + d'(2n-1)]/(2n+1)$; $\alpha = (z - d')/2$. This leads to $z = 3$ and $\alpha = 1$ for all n in $d' = 1$ whereas $z = 4(2n+1/2)/(2n+1) < 4$ (for all n) in $d' = 2$. The global exponents of Eq. (4.4) are therefore consistent with our MBE numerical simulation results. There are also indications [46] of nonperturbative (logarithmic) singularities for the nonlinear series in Eq. (4.4) which may be responsible for anomalous scaling and multiaffinity observed in our numerical simulations of discrete MBE growth models. The possibility of Eq. (4.4) suffering from nonperturbative “strong coupling” effects in $d' = 1$ was first pointed out in Y. Tu, *Phys. Rev. A* **46**, R729 (1992) even though Tu’s numerical simulations have recently been questioned in V. Putkaradze, T. Bohr, and J. Krug [The Niels Bohr Institute Report No. NBI-95-04, 1995 (unpublished)]. See also Refs. [14,29,30] and particularly Ref. [46] in this context. Further discussion of this issue is well beyond the scope of our paper.

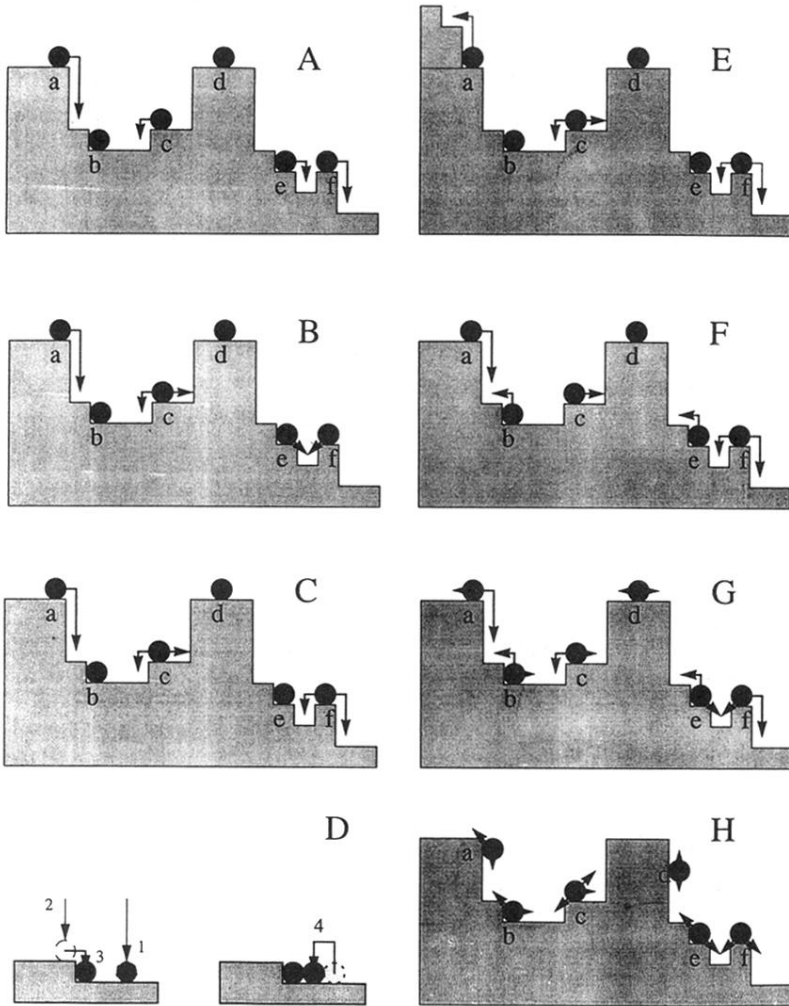


FIG. 1. Schematic configurations defining the growth rules for various models discussed in this paper in $1 + 1$ dimensions. (a) Family model, (b) Wolf-Villain (WV), (c) Das Sarma-Tamborenea (DT), (d) time-dependent hopping (TDH) modification to the DT model, (e) Lai-Das Sarma (LDS), (f) larger curvature model (LC), (g) the minimal MBE model, i.e., the stochastic growth model in solid-on-solid approximation (SOS-MBE), (h) stochastic ballistic deposition model (BD). Atom a in (e), while hopping up in the modified configuration, would not move in DT, and hops down in LC.